
KTH Chemical Science
and Engineering

# Novel oil resistant cellulosic materials

Christian Aulin

Doctoral thesis in Pulp and Paper Technology 2009

Royal Institute of Technology
Department of Fibre and Polymer Technology

Stockholm 2009

TRITA-CHE-Report 2009:57
ISSN 1654-1081
ISBN 978-91-7415-476-4

Akademisk avhandling som med tillstånd av Kungliga Tekniska Högskolan framlägges till offentlig granskning för avläggande av teknologie doktorsexamen fredagen den 4 december 2009, klockan 10:00 i hörsal F3, Kungliga Tekniska Högskolan, Lindstedtvägen 26, Stockholm.


Stockholm 2009, Universitetsservice US-AB

*To my parents*

# Abstract

The aim of this study has been to prepare and characterise oil resistant cellulosic materials, ranging from model surfaces to papers and aerogels. The cellulosic materials were made oil resistant by chemical and topographic modifications, based on surface energy, surface roughness and barrier approaches. Detailed wetting studies of the prepared cellulosic materials were made using contact angle measurements and standardised penetration tests with different alkanes and oil mixtures.

A significant part of the activities were devoted to the development of model cellulosic surfaces with different degrees of crystalline ordering for the wetting studies. Crystalline cellulose I, II and amorphous cellulose surfaces were prepared by spin-coating of cellulose nanocrystal or microfibrillated cellulose (MFC) dispersions, with Langmuir-Schaefer (LS) films or by a layer-by-layer (LbL) deposition technique. The formation of multilayers consisting of polyethyleneimine (PEI)/anionic MFC or cationic MFC/anionic MFC was further studied and optimized in terms of total layer thickness and adsorbed amount by combining Dual Polarization Interferometry (DPI) or Stagnation Point Adsorption Reflectrometry (SPAR) with a Quartz Crystal Microbalance with Dissipation (QCM-D).

The smooth cellulosic surfaces prepared had different molecular and mesostructure properties and different surface energies as shown by X-ray diffraction, Atomic Force Microscopy (AFM) imaging, ellipsometry measurements and contact angle measurements.

The cellulose model surfaces were found to be ideal for detailed wetting studies, and after the surface has been coated or covalently modified with various amounts of fluorosurfactants, the fluorinated cellulose films were used to follow the spreading mechanisms of different oil mixtures. The viscosity and surface tension of the oil mixtures, as well as the dispersive surface energy of the cellulose surfaces, were found to be essential parameters governing the spreading kinetics. A strong correlation was found between the surface concentration of fluorine, the dispersive surface energy and the measured contact angle of the oil mixtures.

Silicon surfaces possessing structural porous characteristics were fabricated by a plasma etching process. The structured silicon surfaces were coated with sulfate-stabilized cellulose I nanocrystals using the LbL technique. These artificial intrinsically oleophilic cellulose surfaces were made highly oleophobic when coated with a thin layer of fluorinated silanes. By comparison with flat cellulose surfaces, which are oleophilic, it is demonstrated that the surface energy and the surface texture are essential factors preventing oil from spreading on the surface and, thus, inducing the observed macroscopic oleophobic properties.

The use of the MFC for surface coating on base papers demonstrated very promising characteristics as packaging materials. Environmental-Scanning Electron Microscopy (E-SEM) micrographs indicated that the MFC layer reduced the sheet porosity, i.e. the dense structure formed by the nanofibers resulted in superior oil barrier properties. Attempts were made to link the procedure for preparation of the MFC dispersions to the resulting microstructure of the coatings, and film porosity and the film moisture content to the resulting permeability properties.

Finally, MFC aerogels were successfully prepared by freeze-drying. The surface texture of the porous aerogels was carefully controlled by adjusting the concentration of the MFC dispersion used for the freeze-drying. The different scales of roughness of the MFC aerogels were utilised, together with the very low surface energy created by fluorination of the aerogel, to induce highly oleophobic properties.

# Sammanfattning

Det övergripande målet med arbetet som beskrivs i denna doktorsavhandling var att preparera och karaktärisera oljeresistenta cellulosamaterial, t.ex. modellytor av cellulosa, celllulosa-aerogeler och papper. Cellulosamaterialen gjordes oljeresistenta genom kemisk och topografisk modifiering baserat på ytenergi-, ytstruktur- och barriäraspekter. Kontaktvinkelmätningar och standardiserade absorptionstester har använts för att studera hur olika opolära vätskor och oljeblandningar sprids på och i cellulosamaterialen.
En stor del av arbetet ägnades åt utveckling av cellulosaytor med olika kristallina egenskaper. Ytorna användes som substrat för att studera oljevätning. Kristallin cellulosa av typ I och II samt amorfa cellulosaytor framställdes med hjälp av spin-coating, Langmuir-Schaefer (LS) och flerskiktsprincipen. Multilager, när t.ex. en laddad yta behandlas omväxlande med motsatt laddade polyelektrolyter/kolloider, har använts för att bygga upp modellytor bestående av polyetylenimin/anjonisk mikrofibrillär cellulosa (MFC) eller katjonisk MFC/anjonisk MFC. Filmernas tjocklek samt den adsorberade mängden karaktäriserades med hjälp av Dual Polarization Interferometry (DPI), Stagnation Point Adsorption Reflectrometry (SPAR) i kombination med Quartz Microbalance with Dissipation (QCM-D).
Cellulosaytorna, med ytråhet på nanometernivå, har olika ytenergier samt kristallina och mikrostrukturella egenskaper. Dessa egenskaper karaktäriserades med röntgen-diffraktion, atomkrafts-mikroskopi (AFM), ellipsometri och kontaktvinkelmätningar.
Fluorerade cellulosaytor användes för att i detalj kunna studera spridningen av olika oljeblandningar. Oljornas viskositet och ytspänning samt cellulosaytornas dispersiva ytenergi var viktiga faktorer som bestämde spridningskinetiken för oljorna. Vidare konstaterades ett samband mellan ytkoncentrationen av fluor, cellulosaytornas dispersiva ytenergier och kontaktvinklarna för oljorna.
Strukturerade kiselytor, med varierande porositet och ytstruktur, har framställts med en plasmaetsningsprocess. De strukturerade ytorna användes som templat för adsorptionen av cellulosa nanokristaller enligt flerskiktsprincipen. Efter att cellulosaytorna belagts med ett tunt lager av fluorerade silaner erhölls markant oljeavstötande egenskaper. Kontaktvinklarna för olika opolära vätskor jämfördes för de strukturerade och plana cellulosaytorna. Genom denna jämförelse konstaterades att ytenergin i kombination med ytstrukturen för celluosaytorna var två mycket viktiga faktorer för att förhindra spridning av de opolära vätskorna.
MFC-dispersioner användes för bestrykning av papper. Svepelektron-mikroskopi (SEM) visade att de bestrukna MFC-skikten bildade en jämn och homogen film. Bestrykningen reducerade porositeten i pappret, vilket i sin tur gav det bestrukna papperet en funktion som oljebarriär. Utifrån de erhållna resultaten diskuteras sambanden mellan egenskaperna hos MFC-dispersionerna och mikrostrukturerna hos beläggningen, samt hur kristallinitetsgraden, filmporositeten och vätebindingarna är relaterat till permeabilitetsgraden hos det bestrukna pappret.
Skräddarsydda MFC-aerogeler preparerades med hjälp av frystorkning. Mikrostrukturen och porositeten hos aerogelerna varierades genom att ändra koncentrationerna för MFC-dispersionerna före frystorkning. Ytstrukturen, och den låga ytenergin från fluoreringen, bidrog till de markanta oljeavstötande egenskaperna hos materialet.

# List of papers

This thesis is based on the following papers:

I. *Wetting kinetics of oil mixtures on fluorinated model cellulose surfaces.*
**Aulin, C.**, Shchukarev, A., Lindqvist, J., Malmström, E., Wågberg, L. and Lindström, T.
Journal of Colloid and Interface Science (2008) 317(2): 556-567.

II. *Build-up of polyelectrolyte multilayers of polyethyleneimine and microfibrillated cellulose studied by in situ dual-polarization interferometry and quartz crystal microbalance with dissipation.*
**Aulin, C.**, Varga, I., Claesson, P.M., Wågberg, L. and Lindström, T.
Langmuir (2008) 24(6): 2509-2518.

III. *Nanoscale cellulose films with different crystallinities and mesostructures - their surface properties and interaction with water.*
**Aulin, C.**, Ahola, S., Josefsson, P., Nishino, T., Hirose, Y., Österberg, M. and Wågberg, L.
Langmuir (2009) 25 (13): 7675–7685.

IV. *Adsorption behaviour, structural and adhesive properties of microfibrillated cellulose-based multilayers.*
**Aulin, C.**, Johansson, E., Wågberg, L. and Lindström, T.
Submitted.

V. *Oxygen and oil barrier properties of microfibrillated cellulose films and coatings.*
**Aulin, C.**, Gällstedt, M. and Lindström, T.
Submitted.

VI. *Design of highly oleophobic cellulose surfaces from structured silicon templates.*
**Aulin, C.**, Yun, S.H., Wågberg, L. and Lindström, T.
ACS Applied Materials & Interfaces, In press.

VII. *Ultra light-weight microfibrillated cellulose aerogels with tunable oleophobicity.*
**Aulin, C.**, Netrval, J., Wågberg, L. and Lindström, T.
Submitted.

Relevant conference presentations not included in the thesis:

1. *Oil/grease resistance for paper/board.*
   Aulin, C., Shchukarev, A., Lindqvist, J., Malmström, E., Wågberg, L. and Lindström, T.
   Poster session, 6th International Paper and Coating Chemistry Symposium, June 7th - 9th 2006, Stockholm, Sweden.

2. *Oil/grease resistance for paper/board.*
   Aulin, C., Shchukarev, A., Lindqvist, J., Malmström, E., Wågberg, L. and Lindström, T.
   Poster session, 233th ACS National Meeting, March 25th – 29th 2007, Chicago, IL, USA.

3. *Preparation, characterization and wetting of fluorinated cellulose surfaces.*
   Aulin, C., Wågberg, L. and Lindström, T.
   Oral presentation by C.Aulin, 235th ACS National Meeting, April 6th -10th 2008, New Orleans, LA, USA.

4. *Adsorption behaviour, structural and adhesive properties of microfibrillated cellulose-based multilayers.*
   Aulin, C., Johansson, E., Wågberg, L. and Lindström, T.
   Oral presentation by C.Aulin, 13th IACIS International Conference on Surface and Colloid Science and the 83rd ACS Colloid & Surface Science Symposium, June 14th - 19th 2009, New York, NY, USA.

## Contribution to the papers

The author's contributions to the appended papers are as follows:

| | |
|---|---|
| Paper I: | Principal author and performed all the experimental work, except for the XPS measurements (performed by Dr. A. Shchukarev). |
| Paper II: | Principal author and performed all the experimental work, except for the major part of the DPI measurements (performed by Dr. I. Varga). |
| Paper III: | Principal author and performed all the experimental work, except for the QCM-D measurements (performed by Dr. S. Ahola) and Small incidence angle X-ray diffraction measurements (performed by Y. Hirose). |
| Paper IV: | Principal author and performed all the experimental work, except for the AFM force measurements (performed by E. Johansson). |
| Paper V: | Principal author and performed all the experimental work, except for the oxygen permeability measurements (performed by Dr. M. Gällstedt). |
| Paper VI: | Principal author and performed all the experimental work, except for the fabrication of the structured silicon surfaces (performed by Dr. S.H. Yun). |
| Paper VII: | Principal author and performed all the experimental work. |

# Contents

# 1 Objectives

The primary objective of this work was to formulate a detailed description of the factors controlling the wetting of cellulosic materials by different types of alkanes and oil mixtures. These factors are of great importance since several paper products, such as paper/board for pet, bakery and fast food products, are exposed to different types of oil/grease. By gaining fundamental knowledge of the factors controlling oil resistance, this work aims at creating a potential base for the development of future products for preparing papers with a controlled degree of oil resistance.

The main purpose of **paper I** was to characterise the contact angle and wetting kinetics of oil mixtures on fluorinated cellulose surfaces, and to relate these results to the surface concentration of fluorine and dispersive surface energy of the surfaces. Atomic Force Microscopy (AFM) and X-ray Photoelectron Spectroscopy (XPS), respectively, were used to characterise the surface morphology and the atomic fluorine concentration on the cellulose surfaces.

The primary aim of **papers II, III and IV** was to develop suitable model cellulose surfaces and to use these as substrates for studying the spreading of oils by contact angle measurements. The aim of **paper III** was to prepare cellulose model films with different degrees of crystalline ordering, crystal structure and surface energy and to characterize them using small angle incidence X-ray diffraction, AFM imaging, contact angle measurements and ellipsometry. Attempts were made to link the preparation procedure to the resulting molecular and mesostructure of the films.

In **paper II**, the build-up of a multilayer consisting of polyethylenimine (PEI) and microfibrillated cellulose (MFC) was investigated using two different techniques; Dual Polarization Interferometry (DPI) and Quartz Crystal Microbalance with Dissipation (QCM-D) measurements. The adsorbed amounts of PEI and MFC and the amount of water entrapped by the individual layers in the multilayer structures were estimated by combining results from the two analysis techniques. The results indicate water-rich layers in the multilayer. Since **paper II** showed that it is possible to form multilayers from cationic polyelectrolytes and MFC, the possibility of creating a multilayer using only charge-stabilized MFC dispersions was studied in **paper IV**.

The aim of **paper V** was to evaluate MFC as a potential agent for application in packaging materials and bioplastics. Two papers with different air permeabilities were coated with MFC to study the conditions required to obtain a packaging material with a good oil barrier. The coated papers were characterized using Environmental-Scanning Electron Microscopy (E-SEM) and the barrier properties were characterized using air permeability measurements and standardised oil penetration tests. Attempts were made to link the coating and film microstructure with the resulting barrier properties. The moisture content of the films was found to greatly influence the permeability properties.

Surface roughness approaches were used in **papers VI and VII** in order to obtain highly oleophobic (e.g. $\theta_{\text{castor oil}} >> 90^{\circ}$) cellulose materials. In **paper VI**, structured silicon templates were coated with nanocrystals of cellulose and thereafter modified with a thin layer of a fluorinated silane. The structured cellulose surfaces were found to have highly non-wetting properties against alkanes such as hexadecane and decane with surface tensions as low as 27.5 and 23.8 mN/m, respectively. In **paper VII**, the surface textures of MFC aerogels were simply altered by changing the concentration of the MFC dispersions before freeze-drying. By modifying the MFC aerogel using chemical vapour deposition of a fluorinated silane, non-wetting properties were obtained.

# 2 Introduction

## 2.1 Structure and chemistry of cellulosic fibers

The basic units of paper materials are the individual fibers and their major constituting building blocks cellulose, hemicelluloses and lignin. Cellulose is the load-bearing constituent of the fibers and it is therefore natural to use the organisation of cellulose in the fiber wall as an appropriate starting point for discussing the structure and chemical composition of paper and cellulose materials in general. Cellulosic fibers are heterogeneous in nature and differ between tree species (e.g. hardwood vs. softwood), growth rings (earlywood vs. latewood) and pulping conditions (where the individual fibers are liberated from the wood).
As shown in figure 1, cellulose is a linear homopolymer composed of (1→4)-β-glucopyranose units. The dimer cellobiose is actually the repeating unit of cellulose, but the degree of polymerization is determined based on the number of single anhydroglucose units. Furthermore, the cellulose chain has a direction since the terminal groups on the chain ends are different: a non-reducing end with a closed ring structure and a reducing end with an aliphatic structure and a carbonyl group in equilibrium with a cyclic hemiacetal.[1]

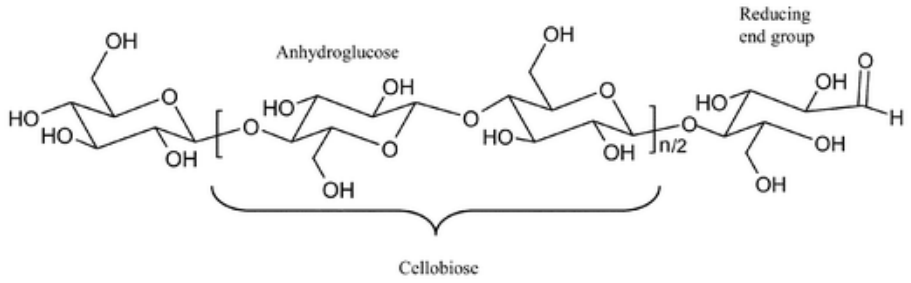


*Figure 1. The structure of cellulose. The anhydroglucose unit is the monomer of cellulose; cellobiose is the dimer. The cellulose chain has a direction, one end being a closed ring structure and the other being an aliphatic reducing end in equilibrium with a cyclic hemiacetal (Kontturi et al., 2006).*[1]

The supramolecular chemistry of cellulose, on the other hand, is a far more complex issue. Four different polymorphs of cellulose are known, named cellulose I, II, III, and IV. Cellulose I is the form found in nature and it occurs in two allomorphs $I_\alpha$ and $I_\beta$. Cellulose II is the crystalline form that emerges after re-crystallization or mercerization with aqueous sodium hydroxide, and it is the thermodynamically most stable crystalline form.[2] Cellulose $III_I$ and $III_{II}$ are obtained by a liquid ammonia treatment of cellulose I and II, respectively. Cellulose IV is a result of heating cellulose III, the transformation usually being only partial. In addition, cellulose is partly amorphous/paracrystalline between the crystallites.[2, 3]

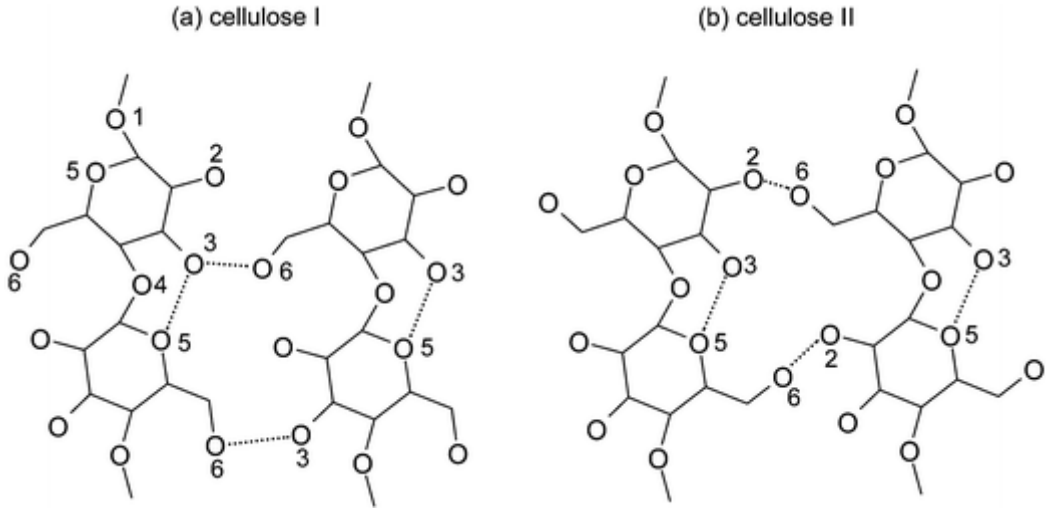


*Figure 2. The major supramolecular distinction between (a) cellulose I and (b) cellulose II (re-crystallized cellulose).[1] The hydrogen atoms are not indicated to emphasize the fact that "free" hydroxyl groups do not really exist in cellulose as all of them are more or less hydrogen bonded.[4] The main intra-chain hydrogen bond is that of O3–H···O5 for both polymorphs. Cellulose I has an O6–H···O3 whereas cellulose II has an O6–H···O2 inter-chain bond (Kontturi et al., 2006).*

The distinction between cellulose I and cellulose II is indicated in figure 2. The dominant intra-chain hydrogen bond in both polymorphs is O3–H···O5, which gives the cellulose chain its rigid, linear shape. The inter-chain bonding is different: in cellulose I, O6–H···O3 dominates, whereas in cellulose II it is O6–H···O2. Furthermore, cellulose II has an antiparallel packing whereas the chains in cellulose I run in a parallel direction.[5-8]

Fibers are built-up of fibril aggregates, which are themselves composed of fibrillar bundles embedded in a matrix of wood polymers. Aside from the individual molecules, these fibrils are considered to be the most basic structure in a cellulosic fiber, and they form the laminate-like layers that ultimately compose the cell wall. The fibrils are believed to be ca. 25-45 Å in diameter and are almost entirely composed of cellulose chains oriented parallel to the length direction. This anisotropy ultimately leads to a high tensile strength and stiffness in the length direction.[9]

The cellulose fibrils are arranged in fibrillar aggregates that are less than 30 nm in diameter and several micrometers in length.[8, 10] These aggregates are held together by an amorphous matrix consisting primarily of lignin and hemicelluloses. Lignin is a relatively highly branched polymer based on phenylpropane units that acts to support the fibril aggregates and prevent buckling.[11, 12] The role of the hemicelluloses has still not been fully resolved, although it appears to couple the cellulose and lignin.[13] The fibril aggregates are arranged in several layers that comprise the fiber cell wall,[14] as shown by the SEM micrograph in figure 3.

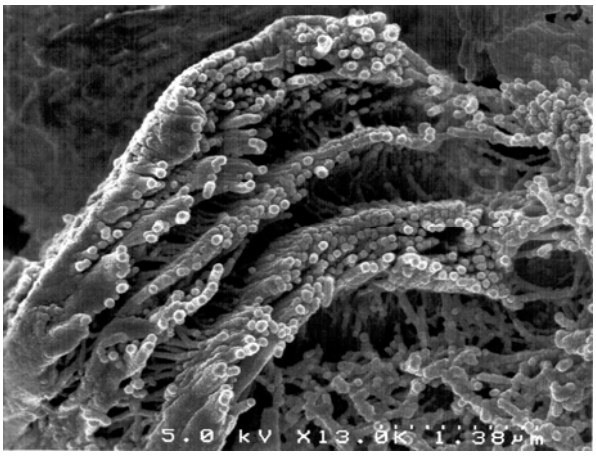


*Figure 3. High-resolution Cryo-FE-SEM micrograph of fractured degraded (i.e. delignified) birch fibres showing the $S_2$ wall composed of concentrically orientated lamellae which at high magnification are composed of characteristic "spaghetti-like" fibril aggregates of fairly uniform size and morphology (Daniel et al., 2004).*[14]

The fiber cell wall consists of three main layers: the middle lamella (M), the primary wall (P) and the secondary wall (S). A sketch showing the arrangement of each layer in the cell wall is presented in figure 4. Although each layer wraps around the cell axis, the different layers can be distinguished by the orientation of the fibrils and the chemical composition. The middle lamella consists of the material which lies between the tracheid cells. The lignin content in the middle lamella varies between 55 and 60%. The primary wall consists of a rough network of fibrils built up of carbohydrates highly encrusted with lignin.[15] The thickness is 0.1-0.3 µm. The secondary wall consists of three layers: the transition $S_1$ region, and the final $S_3$ lamella towards the lumen. All the lamellae are built up of a number of layers. The thickest part of the secondary wall is the $S_2$-layer, which also constitutes ca. 80% of the wood fiber. Here, the fibrils run parallel in a spiral around the fiber at a small angle (10-30º) to the longitudinal direction of the fiber. As previously mentioned, the fibril aggregates are built-up of bundles of cellulose molecules. Some of the cellulose molecules are according to recent studies chemically linked with lignin in the fiber cell wall.[16, 17]

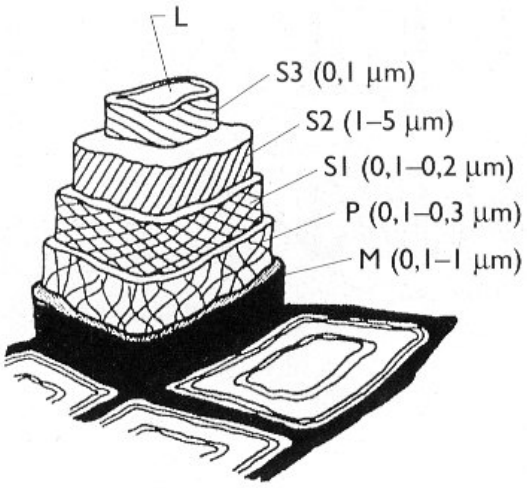

*Figure 4. The structure of the softwood tracheid. The orientation of the cellulose fibrils in the different layers is indicated. M = middle lamella, P = primary wall, $S_1$ = outer layer in the secondary wall, $S_2$ = middle layer in the secondary wall, $S_3$ = inner layer in the secondary wall, L = lumen (the cavity) (Eklund and Lindström, 1991).*[15]

## 2.2 Oil resistant paper

In recent years, there has been an increasing demand for oil resistant paper and paperboards due to the continuously growing packaging markets for food items such as bakery products, pet foods, instant and fast foods.[18] These products are generally packed in paper-based materials and packaging requires a good resistance against staining through oil/fat migration from the product. In general, staining is more of an aesthetic than a product quality problem but this issue still has to be addressed. The staining mechanism for various packaging materials is in general complex and the transportation and storage conditions, such as temperature and humidity, have a major influence on the staining behaviour.[19] Oil resistant paper can in principle be obtained through either a barrier approach; surface coating or mechanical treatment (beating) of the furnish, or a surface energy approach, i.e. application of fluorinated compounds to the furnish or paper.

### 2.2.1 The concept of greaseproof paper – a barrier strategy

Greaseproof paper was invented 100 years ago by the Norwegian engineer Otto Munthe Tobiesen as a replacement for vegetable parchment as a wrapping material for butter and margarine. Today, the concept "greaseproof" implies a paper which in some respects is grease proof and it includes a wide variety of papers used for packaging of fatty products.[20]
Greaseproof papers are mainly produced from highly refined sulphite or sulphate pulp. The wood is mainly spruce or pine, and there are some structural differences between the pulps which affect the production conditions and the barrier properties of the final paper.[21] Beating of cellulose fibers leads to a mechanical degradation and a change in their structure. New surfaces are obtained as a result of external and internal fibrillation of the fibers.[22, 23] External fibrillation involves the removal of the outer layers of the fiber and exposure of the secondary wall. An important consequence of external fibrillation is that new surfaces have been exposed, which increases the possibility of an efficient fiber/fiber joint during drying. Internal fibrillation means that intrafiber bonds are broken and that an internal delamination takes place. The internal structure of the fiber changes and water sorption can take place which is accompanied by a swelling of the fibers. Scallan[24] proposed a "honeycomb" structure, where both tangential and radical cleavage of the lamellae may occur during swelling, as can be seen in figure 5. This structure is also obvious in figure 3. The result is delamination, which makes the fiber more flexible and increases the possibility of contact and joint formation between the fibers. In addition to the fibrillation of the fibers, certain fiber parts and fibrils; fines, are detached from the fiber and occur freely in the fiber suspension. The fine material consists of exposed cellulose fibrils with high anisotropy and this makes a considerable contribution to the strength and barrier properties of the finished paper, by increasing the joint formation between the fibers during consolidation.

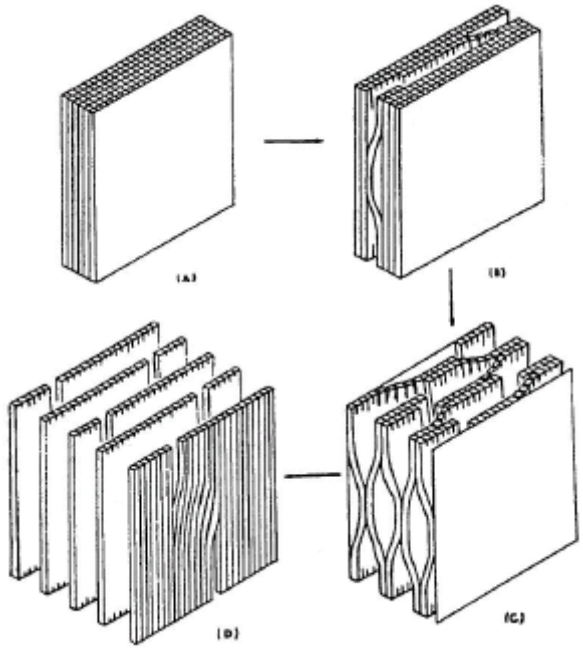

*Figure 5. Progressive swelling of the cell wall leading to internal fibrillation (Scallan, 1978).*[25]

The special properties of greaseproof paper are due mainly to the high degree of beating which creates a large joint forming ability in the fibres, which in turn creates a paper of high density. When calendered at a high temperature, greaseproof papers gain a closed surface structure with a small number of pores,[26] as seen in figure 6. This suggests that greaseproof paper can be an excellent substrate for barrier coating.[21]

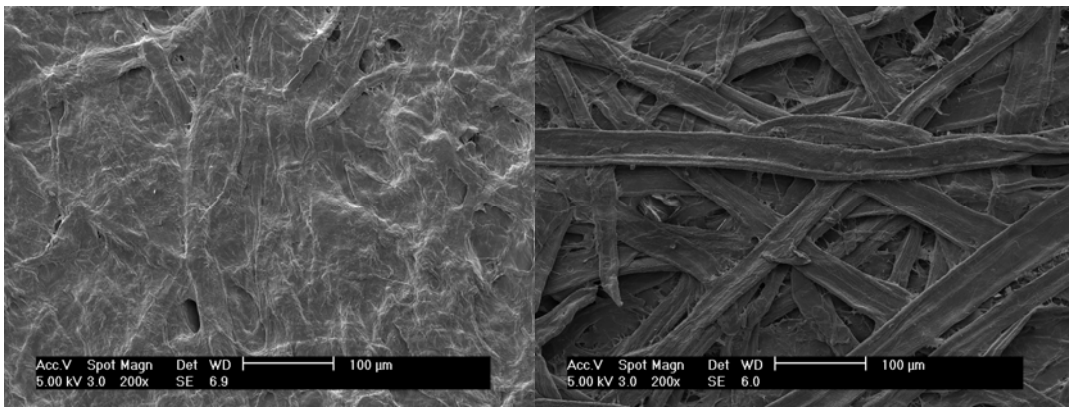


*Figure 6. E-SEM micrographs of (a) greaseproof and (b) unbleached paper. The micrographs clearly show the tightly sealed surface of the greaseproof paper in contrast to the very porous character of the unbleached paper. The absence of macroscopic pores in the greaseproof is due to extensive beating, which produces large amounts of highly hydrated fines and very collapsed fibre walls.*

Most fatty substances used in packaging applications have a very low surface tension, typically in the range of 27 to 32 mN/m,[27] and these substances tend to spread on the paper surface and even penetrate the very fine pores. The speed of penetration is dependent on the

viscosity and surface tension of the oil. Most fats, even solid ones, may contain components of low viscosity which leave fat stains on the reverse side of the porous paper.
Because the oil resistance is achieved by a high degree of beating, this treatment involves high costs in terms of the energy requirements for beating. In addition, an increased degree of beating of the pulp leads to a slower dewatering of the furnish on the wire, and thus a higher moisture content after the press section which leads to a high energy demand in the dryer section. Another, and even more important consequence of the beating, is that the capacity of the drying section will limit the machine speed.[21] Therefore, for both technical and economic reasons, an alternative process to produce oil resistant paper by coating the paper substrate with various barriers is of great interest.

### 2.2.2 Surface coating –a barrier strategy

Surface coating may be an alternative for refining in order to obtain barrier properties and, in addition, papers can be coated with a functional coating. The coatings provide a physical barrier against oil penetration and are therefore sensitive to defects (pinholes) and mechanical abuse. Several coating technologies exist which can provide paper and paperboard with oil barrier properties for packaging and non-packaging purposes. A frequently used method for coating papers is the size press, where a polymer solution is taken up by the paper in the pond (nip) between the size press rolls. Factors that generally determine the size press take-up for polymer solutions have been studied by Dill[28] and Hoyland et al.,[29] and include the viscosity of the polymer solution, the porosity of the paper and the machine speed. Another coating technique, similar to that of the size press, is the Metering Size Press (MSP)[30] on which a pre-metered amount of polymer solution is dosed and where two sides of the paper can be coated simultaneously. Commercially, there are a number of coating techniques for coating paper in order to obtain an oil resistant barrier. Extrusion coating/lamination with melt-streams of various polyolefins, as generated by an extrusion screw, is one of the principal systems for these applications. Others include waxes and wax-metal emulsions,[31] styrene-acrylic copolymers,[32] talc-filled water-based polyacrylate,[33] pigment-filled poly(styrene-butadiene) dispersions,[34] polyvinyl alcohols[35] and montmorillonite/polyethylene-coatings.[36]
However, conventional polymers used in lamination such as polyethylene and polypropylene are based on fossil raw materials, persist for many years after disposal and enhance greenhouse effects when burned.[37] These polymers thus seem inappropriate for applications in which plastics are used for packaging and then disposed of. Furthermore, plastics are often soiled by food and other biological substances, making the physical recycling of these materials impractical. In contrast, biodegradable polymers such as cellulose, starch, chitosan and whey proteins when deposited in bioactive environments degrade by the enzymatic action of microorganisms such as bacteria, fungi, and algae. Their polymer chains may also be broken down by non-enzymatic processes such as hydrolysis. Biodegradable polymers are often derived from plant processing of atmospheric $CO_2$. Biodegradation converts them to $CO_2$, $CH_4$, water, biomass, humic matter, and other natural substances. Biodegradable polymers are thus naturally recycled by biological processes. A sustainable development in the future may require the use of renewable materials. Examples of promising biodegradable polymers that are either in development or already being marketed are shown in figure 7.

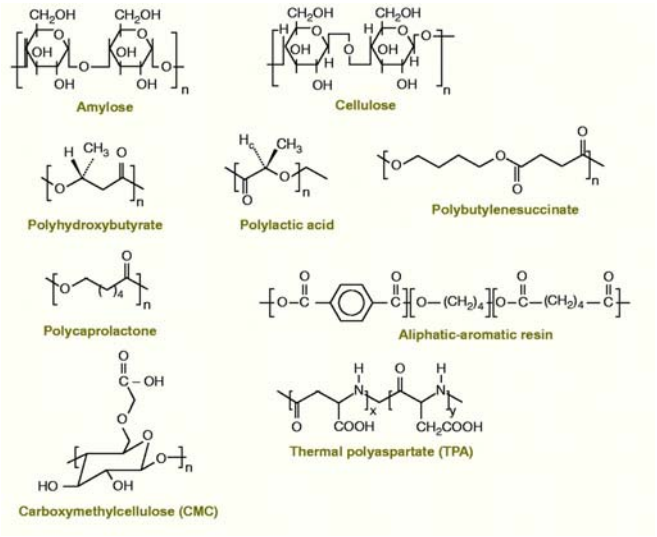


*Figure 7. Structures of selected biodegradable polymers (Gross et al., 2002).*[37]

Although the reviewed coating methods and materials provide a barrier function against oil and fat, these papers are not oleophobic and fatty substances will spread over the film because the surface has a high surface energy. In contrast, paper products treated with fluorinated compounds have low surface energy which provides oleophobicity.[18]

### 2.2.3 Fluorochemistry – a surface energy strategy

Flourinated compounds are not based on any natural products and can be obtained only via multistep synthesis, often through highly toxic intermediates. From a chemical point of view, they are not biodegradable, which is an issue of environmental concern. Despite these drawbacks, fluorocompounds nevertheless attract a lot of attention because of their essential role in many systems that are destined for conceptually new applications in, for example, biotechnology.[38] One of the reasons for the current interest stems from the unique properties exhibited by fluorocarbons. Fluorocarbons substantially surpass hydrocarbons in terms of thermal, chemical, and biological inertness, surface activity (both effectiveness and efficiency), hydrophobicity and oleophobicity. The remarkably strong intramolecular bonds and characteristic low intermolecular interactions are the origin of some of these properties.[39]
In order to create an oil resistant or oleophobic cellulose material, fluorocarbons such as fluorosurfactants or fluoropolymers can be added to the pulp slurry, applied to the paper surface or included in pigment coatings. These types of fluorocompounds have the potential to resist wetting by oils due to their low surface energy (preferably lower than 20 mN/m). The fluorocarbon sizing agents were commercially introduced in the mid-1950s by 3M as a chromium complex sold as Scotchban brand paper size FC-805.[40] They have been widely applied to paper and paperboard, and some publications in the field exist.[26, 27, 38, 40-45] The surface treatment process is the most efficient mode of fluorinated surfactant application and easier to control than the internal application process. In pigment coatings on the outside of boxes or bags, fluorinated surfactants are used to prevent soiling and to maintain the appearance of the package. The oleophobic paper products are most often used where short contact times between the fatty substances and the paper are involved, such as in fast food packaging. Greaseproof papers on the other hand are often used for the more long-term storage of products such as butter and margarine. However, the use of fluorocompounds as oleophobic agents, especially for food contact applications, has been heavily debated for years due to their known toxicity since low molecular weight fluorocompounds can accumulate in

human tissue and have a low biodegradability.[38] The treatment of paper or paperboard used for food and pet food packaging requires Food and Drug Administration (FDA) approval. Consequently, there are only a limited number of companies producing fluorocarbon-treatment chemicals. The market leader (3M with Scotchban) decided in 2000, to stop its production for environmental reasons.[19] Hence, the development of new bio-based and biodegradable additives that impart oil resistance is a very interesting and important research area.

## 2.3 Cellulose model surfaces for oil wetting studies – a surface energy strategy

As already outlined, the cellulosic fibers have a complex composite structure. In addition, they are relatively small, rough, porous and heterogeneous. These features make cellulosic fibers a challenging subject to study. Therefore, to fundamentally study the interactions of cellulose with other solids or liquids, model systems are employed. In this work, cellulose model films were prepared and primarily utilised to study the spreading and wetting of various oils and alkanes. In addition, different types of cellulose model surfaces were used to compare the effects of cellulose molecular structure, film morphology and crystallinity on the resulting surface free energies and wetting by oils.

Cellulose model surfaces have been prepared using different approaches. One of the earliest cellulose model surfaces was reported by Luner et al.,[46] who prepared regenerated cellulose films from viscose and cellulose acetate. Since the introduction of a modern preparation method for smooth, ultra thin films of cellulose by Schaub et al.,[47] the research on cellulose model surfaces has gradually begun to gain more interest.[1] Langmuir-Blodgett (LB) deposition[47, 48] and spin-coating[49] are the most commonly used methods for preparing smooth cellulose model surfaces. Both methods involve dissolving or dispersing cellulose in a liquid before deposition on a solid substrate. Cellulose has been dissolved in solvents such as dimethylacetamide with lithium chloride (LiCl/DMAc)[50-52] or N-methylmorpholine-N-oxide (NMMO),[49, 52-57] resulting in amorphous and semi-crystalline regenerated cellulose II films, respectively. Edgar et al.[58] introduced a method to prepare cellulose model surfaces by spin-coating cellulose nanocrystals suspensions, which gave smooth and highly crystalline cellulose I surfaces.[51, 56, 59-61] Recently, multilayer films of highly anionic microfibrillated cellulose (MFC) and various cationic polyelectrolytes have been prepared by Wågberg et al.[62] These films consist of both crystalline cellulose I and less ordered amorphous or paracrystalline regions.[56]

## 2.4 Cellulose aerogels – a surface roughness strategy

Porous materials with nano- and micro-size pores made from natural polymers are of special interest for medical, cosmetic, pharmaceutical, and other applications where biocompatibility and biodegradability are requested.[63] Porous cellulose aerogels have earlier been prepared from cellulose/calcium thiocyanate solutions by cellulose regeneration followed by freeze-drying or solvent exchange drying.[64] Aerogels of cellulose have also been prepared from NMMO-solutions.[63] Starch-based aerogels reinforced with MFC and pure MFC aerogels have previously been prepared by Svagan et al.[65] and by Pääkkö et al.,[66] respectively, using a freeze-drying technique. Low-density MFC aerogels can thus be prepared from viscous MFC dispersions and in the present work they were utilised as models for studying the relationships between the surface texture of the aerogels and its wetting properties with respect to various

non-polar liquids. By varying the density of the aerogel, see figure 8, the properties can be tailored to meet specific applications.

*Figure 8. MFC aerogels prepared from four different dispersion concentrations; 0.7%, 1.1%, 1.6% and 2% (left to right).*

## 2.5 Wettability of cellulosic materials by non-polar liquids

Because oil repellency is a condition of limited wettability, a discussion of repellency is not possible without reviewing the basic principles of wetting. Wetting of cellulosic surfaces by oils and non-polar liquids involves the displacement of a cellulose-air (vapour) interface by a cellulose-liquid interface. Wetting of a fibrous assembly, such as fibers or papers, is a complex process because of the chemically and physically heterogeneous characteristics of these surfaces and the simultaneous spreading of liquid on the surface of the paper and absorption of the liquid in the pores of the material. Various wetting processes, such as spreading, immersion and capillary penetration, may hence operate simultaneously.
When a drop of oil is placed on a cellulose surface, the drop assumes a shape that appears to be constant and exhibits an angle, θ (figure 9). The angle θ is called the contact angle and is considered to be a characteristic of the particular liquid-solid interaction. Therefore, the equilibrium contact angle serves as an indication of the wettability of the surface by the oil. Many years ago, Young proposed that a liquid drop on a plane solid surface (figure 9) is subject to the following equilibrium situation:[67]

$$\gamma_{sv} = \gamma_{sl} + \gamma_{lv} \cos\theta \qquad (1)$$

where θ is the contact angle of the liquid at the solid-liquid-vapour boundary, $\gamma_{SV}$ is the surface tension of the solid, $\gamma_{LV}$ is the surface tension of the liquid and $\gamma_{SL}$ is the interfacial tension between the solid and the liquid. The surface has to be smooth, homogeneous, impermeable and non-deformable.

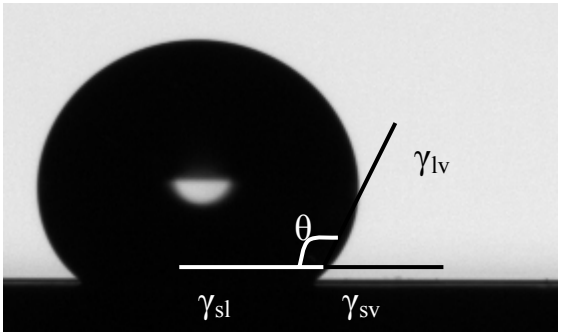


*Figure 9. Equilibrium contact angle (θ) and surface energies involved in spreading.*

Because wood fibers and cellulose materials are not ideal, wetting is complicated by the surface roughness and the heterogeneity. The experimentally observed contact angle is thus an apparent contact angle and a substitution of an apparent contact angle into the equation will give only an approximate results.
There are two possible states when a liquid contacts a rough solid surface; either the liquid is in complete contact with the solid surface or the liquid contacts a composite surface of solid and air and forms a droplet. The relationship between the apparent liquid contact angle on a rough surface (θ*), the roughness coefficient (*r*) and its intrinsic liquid contact angle (θ) has been described by the Wenzel equation:[68]

$$\cos\theta^* = r\cos\theta \tag{2}$$

and by the Cassie−Baxter equation:[69]

$$\cos\theta^* = f_1\cos\theta - f_2 \tag{3}$$

where $f_1$ is the surface area of the liquid in contact with the solid divided by the projected area and $f_2$ is the surface area of the liquid in contact with air trapped in the pores of the rough surface divided by the projected area.
The conditions for highly non-wettability, (θ* >> 90°) can be realized only in the case of a composite interface where the solid-liquid contact area ($f_1$) is low. However, for low surface tension liquids with θ < 90°, the fully wetted or Wenzel state represents the thermodynamic equilibrium state while the composite interface or the Cassie−Baxter state is metastable when θ > 90° ,[70-74] representing a local minimum in the overall Gibbs free energy. Thus, for liquids, the transition from a composite interface to a fully wetted interface is irreversible, and typically this transition leads to a loss of the non-wettability.
When considering only the spreading phenomenon, the spreading coefficient S is defined as:

$$S = \gamma_{sv} - \gamma_{sl} - \gamma_{lv} \tag{4}$$

A positive spreading coefficient predicts that the liquid will spread spontaneously over the cellulose surface and wet it. Qualitatively, the surface free energy of the cellulose surface, $\gamma_S$, should be made as small as possible if spreading and wetting are to be discouraged.
As previously stated, the phenomenon of liquid penetration into a porous medium such as paper is complex and modelling of the non-uniform pore structure in paper is difficult.
Assuming that the liquid exists in a cylindrical capillary with a constant radius *r* and the attraction forces are such that a defined contact angle θ exists between the liquid and the capillary wall, the capillary pressure $P_C$ is given by:

$$P_c = \frac{2\gamma_l \cos\theta}{r} \tag{5}$$

which is called the Laplace equation.
The capillary pressure is counteracted by the pressure drop due to the flow resistance, $P_F$, which can be calculated according to the Hagen-Poiseulle law:

$$P_F = \frac{8\eta v l}{r^2} \tag{6}$$

where $l$ is the penetration length, $v = dl/dt$ is the rate of penetration and $\eta$ is the viscosity of the liquid. The pressure equilibrium at the liquid front is thus:

$$P_E + P_C = P_F \tag{7}$$

where $P_E$ is the external pressure. Substitution of the expression for $P_C$ and $P_F$ in equations 5 and 6 respectively yields:

$$P_E + \frac{2\gamma_l \cos\theta}{r} = \frac{8\eta(dl/dt)l}{r^2} \tag{8}$$

The solution to this differential equation shows that the penetration distance is proportional to the square root of the time, $\sqrt{t}$

$$l = \sqrt{\frac{2r\gamma\cos\theta + P_E r^2}{4\eta}}\sqrt{t} \tag{9}$$

This equation is known as the Washburn equation.[75] Assuming that the paper consists of a bundle of capillaries of a certain size, the Washburn equation can be used to understand the critical parameters that affect the sizing phenomenon. Among these parameters, γ and η are the properties of the penetrating liquid. To slow down penetration, low γ, r and $P_E$ values and large θ and η values are desirable.
There are several standardised methods for testing oil repellency. Some of them, such as DIN 53116 or ISO 5634, measure the time it takes for a standardised grease to penetrate a paper. Others use a standardised test oil. For instance, Tappi 454 uses turpentine oil. These tests measure the time between placing a fatty substance on a paper and the appearance of grease spots on the reverse side of the paper. The advantage of the DIN and ISO methods is that they are realistic; they also use actual fatty substances. Their disadvantage is the time the testing requires, sometimes several days. The Tappi method is quicker but is also less realistic since it uses a substitute substance and involves no pressure. It always provides very good results when testing a porous paper treated with fluorochemicals.[20]
Another fast indirect method has been developed by the 3M Company. This method is published as Tappi 557 and is often referred to as the Kit-test. The test uses a series of mixtures of castor oil, toluene and heptane. As the ratio of oil to solvent is decreased, the viscosity and surface tension also decrease, making successive mixtures more difficult to holdout. The performance is rated by the highest numbered solution which does not darken

the paper after 15 seconds. The method is useful for fluorochemical-treated papers,[41, 43, 44] but it is not applicable to pure greaseproof papers.

A great deal of fundamental work has been performed in the area of water interactions with solid substrates[72, 76-84] such as paper surfaces.[85] However, despite the fact that there are many applications, little fundamental research work has been done in the area of oil resistance of cellulosic materials..[21, 27, 41, 44, 86, 87] Starting with materials known to give good oil resistance, like fluorochemicals deposited on various cellulose substrates (as models for paper), detailed descriptions of the factors controlling the wetting of oils can be studied. Thus, more fundamental knowledge will be gained that may in the long term be used to develop new products where the oil resistance can be controlled/adjusted to different degrees.

# 3 Experimental

An overview of the most important experimental aspects of the thesis is given here. For more thorough descriptions, the reader is referred to the individual papers.

## 3.1 Chemicals

**Anchoring polyelectrolytes**
In the experiments reported in papers I - IV and VI, polyethyleneimine (PEI) was adsorbed onto silica as an anchoring polyelectrolyte for cellulose or used as the cationic polyelectrolyte in the multilayers incorporating MFC or cellulose nanocrystals. PEI with a mean molecular weight of 60000 g/mol (according to the supplier) was purchased from Acros Organics in the form of a 50 wt % aqueous solution. PEI is a highly branched cationic polyelectrolyte containing primary, secondary and tertiary amino groups with a ratio of 1:2:1.[88] The PEI is practically neutral at pH > 10.5, whereas it possesses a considerable charge density in the neutral and acidic pH range.[89, 90]
Some the cellulose model surfaces were prepared in collaboration with other research groups which led to the use of several different anchoring polymers. In paper III, the substrates used for the Langmuir-Schaefer-film preparation were either QCM-D crystals, which were spin-coated with polystyrene by the supplier (Q-Sense AB, Västra Frölunda, Sweden), or silicon wafers which were hydrophobized by immersion of 0.04% dichloromethylsilane (> 99%, Sigma Aldrich). 3-aminopropyltrimethoxysilane (APTS, 97%, Sigma Aldrich) was used as an anchoring polymer to improve the coverage of the silicon surface with low-charged (LC) microfibrillated cellulose.

**Microfibrillated cellulose**
Cellulose fibrils are the major reinforcing constituent of plant fiber cell walls. The Young's modulus of the cellulose I crystal can be as high as 220 GPa.[91] Microfibrillated cellulose (MFC) obtained by disintegration of the plant fiber cell wall[92, 93] has an average width in the range of 20 nm, is several micrometers in length, and has a high specific surface area. The average microfibril diameter depends on the plant source, pre-treatment[62, 94] and disintegration procedure.
The MFC used in this work was prepared at Innventia AB, Stockholm, with the aid of a high-pressure homogenization technique similar to a procedure described[92, 93] but with a different high pressure homogenizer and new pre-treatments of the wood fibres. The pulp was a commercial sulfite softwood-dissolving pulp from 60% Norwegian spruce (Picea abies) and 40% Scots Pine (Pinus sylvestris), with a hemicellulose content of 4.5% and a lignin content of 0.6% (Domsjö Dissolving Plus, Domsjö Fabriker AB, Sweden). Three types of MFC materials; low-charged (LC-MFC), and both cationic and anionic high-charged (HC-MFC), were used. The LC-MFC was pre-treated with enzymatic hydrolysis and mechanical refining before disintegration of the fibers in the high-pressure homogenizer. The preparation of the LC-MFC is described in detail by Pääkkö et al.[94] The anionic and cationic HC-MFC´s were prepared by a carboxymethylation pre-treatment[62] or by reacting the pulp with N-(2,3 epoxypropyl)trimethylammonium chloride, respectively, before the homogenization step. For the experiments in papers I - III, the once-homogenized fibrils were further dispersed by sonication using a titanium microtip probe (3 mm tapered microtip with VCX 500 Ultrasonic processor, Sonics, US) followed by centrifugation for two hours at 8000 g.[62] In papers IV, V and VII, the fibrils were passed ten times through the homogenizer, each with a subsequent dilution step, in order to ensure a proper dispersion of the microfibrils. The surface charge

density of the cationic and anionic MFC´s at pH 7.2 and 6.5, respectively, was found to be ca. 322 and 426 μeq/g using polyelectrolyte titration.[95]

**Cellulose model surfaces**

Cellulose model surfaces were prepared in order to study the wetting mechanisms of various oils (paper I) and to determine the surface free energy (paper III) of the substrates. The prepared films were as follows:

*NMMO films:* A commercial sulfite softwood-dissolving pulp (Domsjö Dissolving Plus, Domsjö Fabriker AB, Sweden) was used as raw material for preparing amorphous and regenerated cellulose II films. The regenerated cellulose II surfaces were prepared using PEI as anchoring polyelectrolyte on a silica surface. The cellulose dissolved in N-methylmorpholine-N-oxide (NMMO, 97%, Sigma Aldrich) and diluted by dimethyl sulfoxide (DMSO, 99.9%, Sigma Aldrich) was then spin coated on top of the anchoring layer. The temperature and concentration can be used to affect the viscosity of the dissolved cellulose suspension, which is what determines the film thickness and the surface roughness upon spin coating.[55]

*LiCl/DMAc-films:* Cellulose was dissolved in lithium chloride/dimethylacetamide (LiCl/DMAc) in order to prepare amorphous cellulose films. The cellulose dissolution was performed according to Berthold et al.[96] and the films were then prepared according to Eriksson et al.[50]

*Cellulose nanocrystal films:* A colloidal suspension of cellulose I nanocrystals was prepared by acid hydrolysis of a dissolving grade pulp by a previously described method[97] (kindly provided by Prof. Derek Gray, McGill University, Montreal, Canada). The colloidal suspension of cellulose nanocrystals was used to prepare cellulose I surfaces using a modified procedure based on the method of Edgar and Gray.[58] A 1% w/w of this colloidal suspension of cellulose I nanocrystals was spin-coated onto a silica wafer pre-treated with PEI. The films were subsequently heat-treated to ensure that the films did not delaminate upon exposure to an aqueous electrolyte solution.

*Langmuir-Schaefer-films:* Trimethylsilyl cellulose (TMSC) was deposited on dichloromethylsilane pre-coated silicon wafers using the horizontal LS-deposition technique. The preparation of films is described in detail by Tammelin et al.[98] Prior to use, TMSC deposited on the pre-coated crystal was converted to cellulose by desilylation using hydrochloric acid vapour.[47, 48]

*LC-MFC films:* APTS was used as an anchoring substance for the LC-MFC film preparation. The model films were then prepared by spin-coating the fibril dispersion onto the substrate. The spin-coated surfaces were rinsed with water and heat-treated in an oven. The preparation of the nanofibril films is presented in more detail by Ahola et al.[99]

*PEI/HC-MFC and PEI/cellulose nanocrystal films:* The multilayer films of HC-MFC were formed by simple dipping. All films were deposited on a precursor layer of PEI. The dipping time for MFC was 20 minutes and this was followed by two consecutive five-minute dips in Milli-Q water in order to rinse off the excess MFC. When a layer of PEI was applied, the dipping time was ten minutes and the rinsing procedure was the same. The sequence used in these experiments was hence; formation of an initial layer of PEI and then a MFC layer followed by alternating PEI and MFC dipping.[62] The same procedure was used for the build-up of PEI/cellulose nanocrystals mutilayers. The PEI/HC-MFC multilayer films were used for surface free energy determinations and oil wetting studies, respectively, whereas the PEI/cellulose nanocrystals were used for the build-up of cellulose films on structured silicon templates.

**Microfibrillated cellulose aerogels**

The MFC aerogels were prepared using freeze-drying and the MFC content was changed from 0.0031% to 3.13%. Prior to use, MFC dispersions with concentrations < 3.13% were prepared by diluting a 3.13% MFC dispersion and these were then re-disperse and mix (8000 rpm) the dispersion using an Ultra Turrax mixer (D125 Basic, IKA, Germany) for 5 min. Cylindrical polydimethylsiloxane (PDMS) cups were used as moulds for the preparation of the aerogels. The aqueous gel was placed in the mould and the mould was quickly plunged into liquid nitrogen. Thereafter, the frozen sample in the mould was transferred into a vacuum oven at -52 °C (Labconco FreeZone 6, US), and the sample was kept frozen during the drying at a pressure of 0.016 mbar. The freeze-drying was typically finished within 24 h.

**Fluorocompounds**

Various fluorinated compounds have been used for oleophobization and for adjusting the surface energy of the cellulose surfaces studied.

An anionic fluorosurfactant, perfluorooctadecanoic acid (95%), $C_{17}F_{35}COOH$ (Fluorochem Ltd, UK), was used as cellulose surface coating in paper I. The flurosurfactant was dispersed in Milli-Q water during stirring and made up to a stock solution of 200 mg/l. The pH of the dispersion was adjusted to 7 with 0.1 M NaOH. A theoretical critical micelle concentration (CMC) of ca. 0.02 mg/l was obtained for perfluorooctadecanoic acid by extrapolating CMC values associated with lower aliphatic perfluorinated organic acids ($C_XF_{2X+1}COOH$).[38] However, the CMC at 80 ºC has been determined to be 8 x $10^{-5}$ M (~73 mg/l).[100]

The hydroxyl groups of the cellulose surfaces were covalently modified according to a method described by Nyström et al.[101] with a few modifications (paper I). The surfaces were reacted by immersing them in a solution containing 50 - 400 µl pentadecafluorooctanyl chloride (97%, Sigma Aldrich), 205 µl triethylamine (reagent grade, Scharlab S.L.) and a catalytic amount of 4-dimethyl aminopyridine (> 99%, Sigma Aldrich) in 20 ml tetrahydrofuran (> 99.9%, anhydrous, Sigma Aldrich). The reaction was allowed to proceed with continuous mixing for 4 h. The substrates were thereafter washed with THF and ethanol and dried in a vacuum.

Structured cellulose samples were immersed in a coating solution made by dissolving 1 mM (tridecafluoro-1,1,2,2,-tetrahydrooctyl) trichlorosilane (PFOTS, n-$C_6F_{13}CH_2CH_2SiCl_3$, 97%, Sigma Aldrich) into heptane (> 99.5%, anhydrous, Sigma-Aldrich). After about 15 min of coating in this solution, the samples were thoroughly rinsed with heptane and Milli-Q water (paper V).

The functionalization of the HC-MFC aerogels and films was achieved by chemical vapour deposition of the fluorinated trichlorosilane (PFOTS-coating). The aerogels and films were placed in a steel-net above the gaseous phase of the silane and heated at 140 ºC for one hour.

**Oil mixtures and alkanes**

Contact angle measurements were made on the cellulose surfaces with three probe liquids; castor oil (99.5%, Fluka), hexadecane (> 99%, anhydrous, Sigma Aldrich) and decane (> 99%, Sigma Aldrich) with surface tensions of 35.8, 27.5 and 23.8 mN/m, respectively. Three different “Kit test” mixtures, namely 1, 3 and 6, were prepared from castor oil (Sigma Aldrich), toluene (99%, Mallinckrodt Baker) and n-heptane (analytical grade, Mallinckrodt Baker) according to Tappi 559 pm-96. Turpentine oil was used for a standardised oil penetration test according to Tappi 454 om-00. The viscosities of the oil mixtures and of the non-polar liquids were measured using a stress-controlled Bohlin Gemini rheometer as a function of shear rate at 25 ºC. The properties of the three oil mixtures and the alkanes are presented in Table 1.

***Table 1.*** *Properties of oil mixtures and various probe liquids used in the studies.*

| Mixture/liquid: | γ | η* | Volume ratio castor oil : toluene : heptane: |
|---|---|---|---|
| Decane | 23.8[102] | 1.14 | |
| Hexadecane | 27.5[102] | 3.51 | |
| Turpentine oil | 24.4[103] | 1.82 | |
| Castor oil | 35.8[27] | 509 | |
| Kit mixture 1 (castor oil) | 35.8[27] | 509 | 1 : 0 : 0 |
| Kit mixture 3 | 29.3[27] | 121 | 8 : 1 : 1 |
| Kit mixture 6 | 24.1[27] | 19 | 2 : 1 : 1 |

γ = surface energy of the mixture/liquid (mN/m)
η = viscosity of the mixture/liquid (mPas)
* = at a shear rate of 100/s

## 3.2 Methods

In this chapter, the main instruments and methods used during the course of the research are presented. Most of these techniques have been thoroughly described in the literature and hence they are only briefly described here. For more detailed information regarding the techniques, the reader is referred to the individual papers and the references given there.

**X-ray photoelectron spectroscopy (XPS)**
In order to understand phenomena related to the surface chemistry of any material, a knowledge of the surface composition is of large importance. X-ray Photoelectron Spectroscopy (XPS), also known as ESCA (Electron Spectroscopy for Chemical Analysis) provides both elemental and chemical state information of surfaces virtually without restriction on the type of material which can be analysed. XPS spectra are obtained by irradiating a material with a beam of X-rays while simultaneously measuring the kinetic energy and the number of electrons that escape from the top 1 to 10 nm of the material being analyzed. This makes XPS an appropriate tool for the studying of, for example, thin cellulose films deposited on silicon substrates. A more thorough description of the technique can be found elsewhere.[104]
In the current work, XPS (Kratos Axis Ultra DLD, Kratos Analytical Ltd., Manchester, UK) was used to determine the atomic surface concentrations of the elements on pure and fluorinated cellulosic surfaces (papers I, IV, VI and VII). The peak intensities and hence the relative amounts of the elements on the surface were determined by integrating the areas under the peaks.

**Atomic Force Microscopy (AFM) – imaging**
The function of the Atomic Force Microscope for imaging can be described as follows: A cantilever, with a sharp tip, is brought into contact with a substrate mounted on a piezo electric tube, which expands and retracts in response to an applied voltage. A laser beam is focused on the cantilever and reflected via a mirror to a photo-sensitive detector. The substrate is then moved in the x-y direction and the cantilever follows the surface topography through the z-direction movement of the piezo electric tube. A feed-back loop ensures that the cantilever is kept at constant oscillation amplitude and the z-direction movement of the piezo electric tube is recorded.[105, 106]

In this study, the AFM technique (Nanoscope IIIa, Veeco, Santa Barbara, US) was used to examine the morphology and surface roughness of the cellulose films. For further details about the AFM measurements, the reader is referred to papers I - IV.

**Contact angle goniometry**

Wetting studies were performed using castor oil, hexadecane, decane and several oil mixtures on pure and fluorinated cellulose surfaces (papers I and VI). Surface free energy measurements (paper III) were made for various cellulose films with different structures and different degrees of crystallinity, using three probe liquids: Milli-Q water, glycerol (99%, Sigma Aldrich), and diiodomethane (99%, Sigma Aldrich). The oleophobic properties of the fluorinated MFC aerogels were measured using contact angle measurements with castor oil and hexadecane (paper VII). The wetting experiments were performed using a Contact Angle Meter, CAM 200 (KSV Ltd., Helsinki, Finland). The heart of the instrument is the high performance digital camera (CCD-camera) capable of taking 100 pictures per second. The software delivered by the instrument manufacturer calculates the contact angle based on a numerical solution of the full Young-Laplace equation. The surface energies were calculated from the contact angle data at equilibrium by the Van Oss method,[107, 108] For further details about the contact angle measurements, the reader is referred to the papers I, III, VI and VII.

**Quartz crystal microbalance with dissipation (QCM-D)**

The QCM-D technique makes it possible to follow the adsorption on the surface of the quartz crystal sensor by monitoring the resonance frequency ($\Delta f$) of the crystal and the dissipation ($\Delta D$) of the oscillation energy. These quantities change during adsorption onto the crystal due to changes in the viscoelastic properties of the medium in the vicinity of the active surface. The build-up and viscoelasticity properties of various multilayers incorporating MFC were studied using a QCM-D equipment supplied by Q-Sense AB (Västra Frölunda, Sweden) (papers II and IV). The instrument is described in detail by Rodahl et al.[109] and figure 10 shows a diagram of the technique.

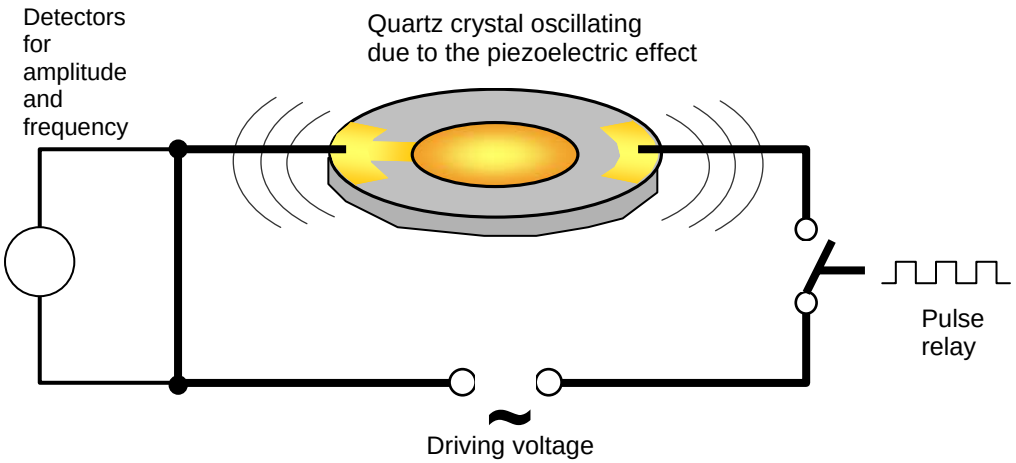


*Figure 10. Principle of QCM-D analysis. A quartz crystal is vibrating at its resonance frequency, driven by a pulsed sinusoidal voltage. When the pulse is shut off, the amplitude decay is measured. The relative loss in amplitude during a period of oscillation is defined as the dissipation factor (Enarsson, 2008).*[110]

**Stagnation point adsorption reflectometry (SPAR)**

Reflectometry is an optical technique which measures changes in intensity of reflected light. When equipped with a liquid cell, it is suitable for adsorption studies at solid/liquid interfaces. Reflectometry require a proper optical model in order to relate the measured quantities to the adsorbed amount.

A continuous flow of the absorbent is added via the sample inlet, directed perpendicularly towards the silica surface. In the projection of the inlet on the silicon surface an infinitesimal point without convective flow is found. This is defined as the stagnation point at which the mass transport is limited by diffusion through a thin boundary layer. A polarized laser beam enters through a glass prism and is reflected by the silicon oxide surface onto a detector. When material is adsorbed onto the surface, the refractive index of the surface layer changes, and the reflection of the incident laser beam is thus altered to some extent. For a more thorough description of the technique, the reader is referred to the original publications by Dijt et al. [111, 112] A schematic diagram of the instrumental setup is presented in figure 11.

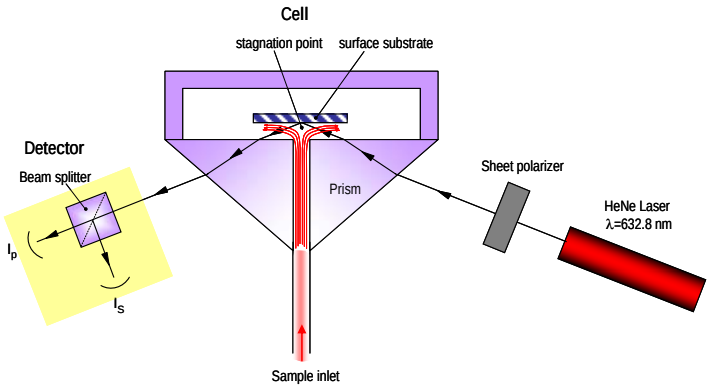


*Figure 11. Schematic drawing of the stagnation point adsorption reflectometer (Enarsson, 2008).*[110]

Polyelectrolyte/MFC adsorption experiments (paper IV) were conducted using a Stagnation Point Adsoption Reflectometer (SPAR) from the Laboratory of Physical Chemistry and Colloid Science, Wageningen University, The Netherlands.

**Ellipsometry**

Ellipsometry is an optical technique which measure changes in the polarisation of light reflected from a sample surface. As in the case of reflectomerty, ellipsometry requires a proper model in order to relate the measured quantities to thickness. The theory of optical reflection is explained in detail in many textbooks, for example by Azzam and Bashara.[113]

In this thesis work, a manual nulling photoelectric ellipsometer (Type 43702-200E, Rudolph Research Analytical, NJ, USA) was used to determine the film thickness of various cellulose films (paper III). By combination of positions of polariser and compensator, linear polarised light is created so that the phase shift between its components disappears after reflection from the samples. The resulting linear polarised light can be extinguished by the analyser. The combination of the positions of the polariser and analyser gives the minimum intensity at the detector. With experimental values of $\Psi$ and $\Delta$, expressed for the analyser and polariser, respectively, the thickness of the adsorbed film can be determined by an iterative procedure, provided that the refractive index of the film is known.

**Dual polarization interferometry (DPI)**

The DPI (Farfield Group Ltd., Cheshire, UK) is a new technique that was used to study the adsorption behaviour of multilayers of PEI and MFC (paper II). DPI is a technique which is able to measure changes in both thickness and refractive index of an adsorbed layer *in situ*. It has previously been used to measure the adsorption of proteins or DNA,[114-117], and for polypeptide multilayer build-up.[118] A detailed description of the instrument is given by Swann et al.[119] and Freeman et al.[120]

The heart of the instrument is the substrate surface, which is a sandwich chip structure of two horizontally stacked waveguides, made of silicon oxynitride, separated by an insulation layer (figure 12).

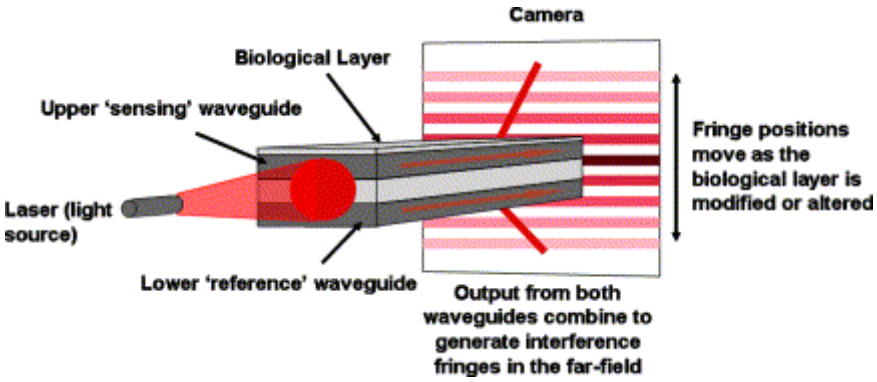


*Figure 12. Schematic drawing of the DPI setup and the waveguide chip structure. The figure is reproduced with the permission of the Farfield Group Ltd.*

A laser beam which can be switched between the two plane-polarized states, transverse electric (TE) and transverse magnetic (TM) (one parallel and one perpendicular to the surface), is used as the light source. The plane-polarized laser light is focused on the short end of the surface, where it splits and travels separately through the two waveguides (sensing and reference). As it emerges on the other side of the chip, the two signals diffract and interfere with each other, and this interference can be detected by a CCD-camera as a fringe pattern. The evanescent field emitted by the sensing waveguide into the solution is affected by changes in the index of refraction in close proximity to the surface, and therefore also by adsorption onto the surface. Hence the light propagating through the sensing waveguide is somewhat altered, usually slowed down, in relation to the light travelling through the reference waveguide, and this creates a phase difference between the two signals. The phase difference can be determined from the shift in the fringe pattern. Since the refractive index of the reference waveguide remains unchanged, the change in effective refractive index relates only to the changes in refractive index close to the sensing waveguide. Shifts in the fringe pattern are recorded continuously for both polarizations, and for both states the calculated effective refractive index can satisfy a continuous range of thickness and refractive indices for an adsorbed film. By combining the results from both polarizations, a unique solution for the thickness and the refractive index can be obtained.

**Scanning electron microscopy (SEM)**

The structures of the MFC films and aerogels (papers V and VII, respectively) and of the cellulose nanocrystal films (paper VI) were studied with a Hitachi S-4800 Field Emission-Scanning Electron Microscope (FE-SEM) to obtain secondary electron images. The specimens were fixed on a metal stub with colloidal graphite paint and coated with a 3 nm thick gold/palladium layer using a Cressington 208HR High Resolution Sputter Coater.

To analyze the surface texture of MFC-coated and uncoated papers (paper V), a Philips XL30 ESEM-FEG (Environmental Scanning Electron Microscope-Field Emission Gun) was used. The surfaces of the paper samples were coated with a thin conducting layer of gold and imaged in a high-vacuum mode using an SE detector (Secondary Electrons).

**Paper coating and air permeability measurements**

A kraft paper (wrapping paper) and a greaseproof paper with different air permeance levels were used as base papers for MFC-coating. The papers were made from softwood pulp and produced by Nordic Paper AB, Säffle, Sweden. The kraft paper was unbleached and contained no pigment filler. The base papers were coated on a bench scale with an aqueous anionic MFC dispersion having a concentration of 0.85 wt%. The bench-scale coatings were performed using a rod coater for sheets, K101 Control Coater (RK Print Coat Instruments Ltd., Herts, UK).

The air permeability, U (m/Pa s), usually used for quality control in the production of greaseproof paper, was used in this work to characterize the MFC-coated papers (paper V). The air permeability was measured according to SCAN-P 26:78, and it is given by the expression:

$$U = \frac{q}{A\Delta p} \tag{10}$$

where $q$ is the air flow ($m^3/s$), $A$ is the area of the paper sample ($m^2$) and $\Delta p$ is the difference in the air pressure (Pa) between the two sides of the paper.

**Oxygen permeability measurements**

In paper V, free-standing MFC films were prepared to examine their potential for use as a barrier coating with low oxygen permeability (OP). The oxygen transmission rate (OTR) was determined by using a Mocon Ox-Tran Model 2/20 apparatus equipped with a coulometric oxygen sensor (Mocon, Minneapolis, USA). The MFC films were mounted in an isolated diffusion cell where one side of the film is exposed to oxygen (99.95%) at atmospheric pressure. The oxygen which permeates through the sample is transported to a coulometric sensor, where the amount of oxygen is measured. The OTR was normalized with respect to the thickness to yield an OP value.

# 4 Results and discussion

The following section is a summary of the results in the different papers. Due to their close relationship, the results from the individual papers are presented together.

## 4.1 Design of smooth cellulose surfaces (papers II - IV)

In this work, non-modified and fluorinated cellulose model surfaces have been proven to be useful tools on which to study the wetting properties of different oils and alkanes. From a comparison of the different cellulose surfaces exhibiting different degrees of crystallinity, crystal structures, nano-structures, it was possible to obtain more information on how these properties affect the wetting properties. The preparation and characterisation of cellulose model surfaces, which is one of the major aspects of this work, was done both in our laboratory and in collaboration with other research groups. The characterisation of the surfaces was of great importance not only to characterize the materials, but also to learn more abut the properties and fundamentals of many of the surfaces consisting of multilayers incorporating nanocellulose fibrils.

### 4.1.1 Preparation of cellulose surfaces; morphology, degree of crystallinity and surface energy

AFM height imaging was used to determine the morphology and surface roughness of the cellulose films (figure 13). Phase images were generated to provide additional structural information, as a consequence of variations in the cellulose material properties such as adhesion, friction and viscoelasticity.[121, 122] AFM images of the LC-MFC and the PEI/HC-MFC multilayer films shows fibrillar network structures with very low rms roughness values. Compared with the LC-film, the PEI/HC-MFC films formed denser structures, where the surfaces are fully covered with fibrils. The carboxymethylation pre-treatment makes the fibrils highly charged and easier to liberate,[62] and this results in smaller and more uniform fibril dimensions (10 to 15 nm) compared to the LC-MFC, where the fibril width was 10 - 30 nm, as measured directly from the AFM height image. A possible broadening effect due to the geometry of the tip has not been considered.
Figure 13 also shows images of the film prepared from the LiCl/DMAc solvent. The film exhibited a non-fibrillar spherically shaped structure in the nanometer scale totally covering the silica substrate. The height and phase mode images of cellulose II surfaces regenerated from NMMO-solution indicate fibrillar-like cellulose structures with a width in the range of 10–20 nm overlapping each other.
Cellulose nanocrystals seem to a have a dimension of 15 nm by 100 – 200 nm. The spin-coated cellulose film has a large amount of stiff, randomly orientated nanocrystals adsorbed and no bare silica substrate can be seen.
The measured rms roughness of the LS-deposited cellulose film was 0.5 nm indicating that the surface was very smooth. No mesoscale cellulose structure, comparable to the structure of the other surfaces, could actually be seen in the images.

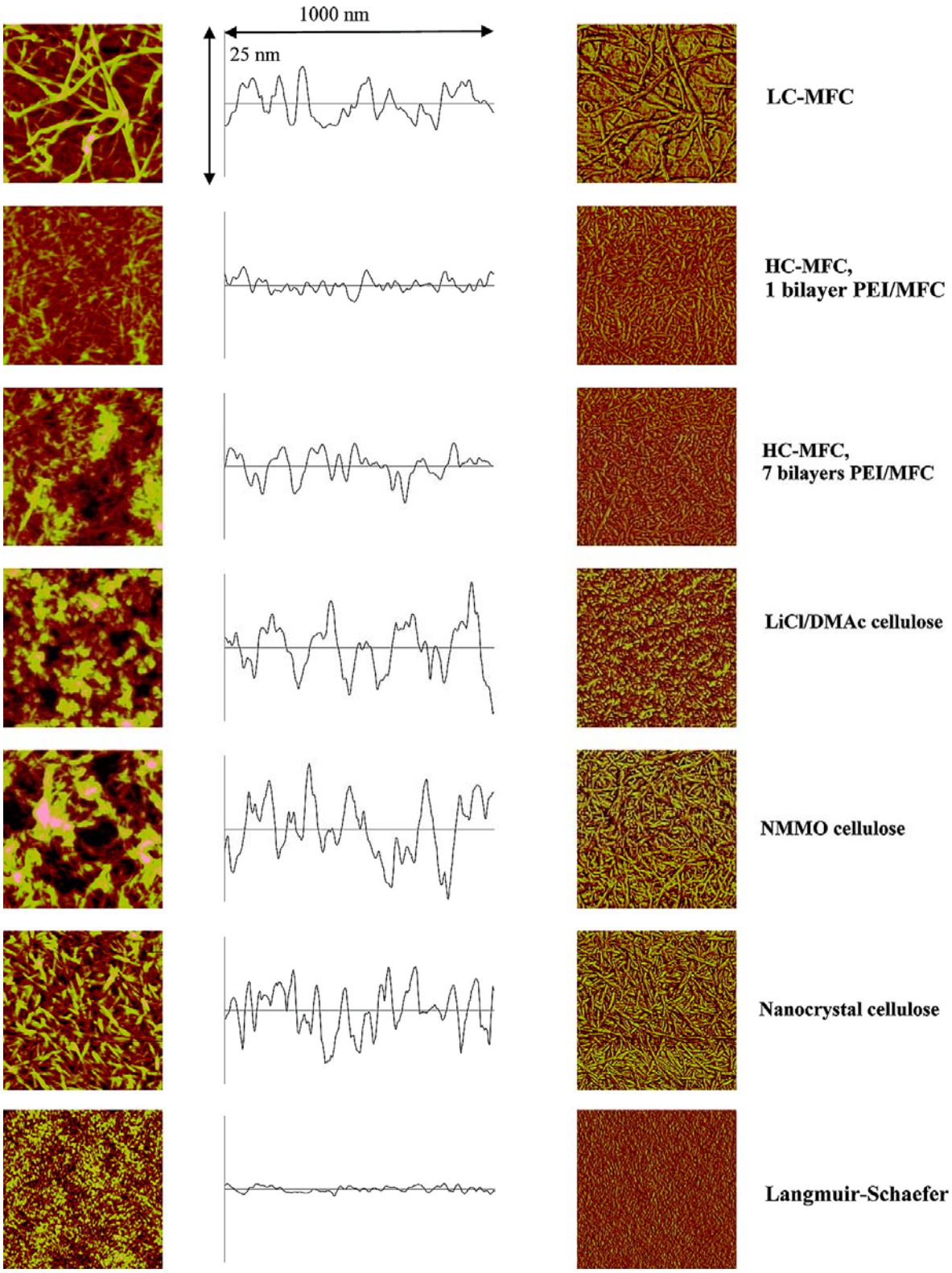


*Figure 13. AFM height (left) and phase (right) images of the cellulose films on silica. The scanned surface areas were 1 μm² and the z-ranges are 25 nm for the LC-MFC, HC-MFC and nanocrystal surfaces, 40 nm for the NMMO and LiCl/DMAc surfaces and 3 nm for the LS surfaces. Typical height profiles are shown in the middle, all with a z-range of 25 nm.*

To evaluate the ability of the cellulose surfaces to interact with various liquids, the surface energies and their contributing components were determined through contact angle

measurements with water, glycerol and methylene iodide.[107, 108] The contact angle data and the surface energies obtained are presented in Table 2.

***Table 2.*** *Total surface energies of the cellulose films and their respective polar and dispersive components, calculated from contact angle measurements against water, glycerol and methylene iodide with an uncertainty of ± 2º. Apart from the dispersive and polar component of the total surface energies, the acid/base (electron acceptor/donor) properties are summarized.*

| | Dispersive component ($mNm/m^2$) | Acceptor, $\gamma_s^+$ ($mNm/m^2$) | Donor, $\gamma_s^-$ ($mNm/m^2$) | Polar component ($mNm/m^2$) | Total surface energy ($mNm/m^2$) |
|---|---|---|---|---|---|
| Cellulose film: | | | | | |
| LC-MFC,1 layer | 36.6 ± 1.1 | 4.8 ± 0.4 | 25.2 ± 0.2 | 22.1 ± 2.5 | 58.8 ± 3.6 |
| HC-MFC,1 bilayer PEI/MFC | 40.3 ± 1.0 | 6.2 ± 0.4 | 13.8 ± 0.5 | 18.5 ± 0.6 | 58.8 ± 1.6 |
| HC-MFC,7 bilayers PEI/MFC | 43.9 ± 1.3 | 3.2 ± 0.2 | 14.6 ± 0.4 | 13.6 ± 1.4 | 57.5 ± 2.7 |
| Nanocrystal cellulose | 45.1 ± 0.8 | 2.4 ± 0.1 | 17.2 ± 0.4 | 13.0 ± 0.6 | 58.0 ± 1.4 |
| LiCl/DMAc cellulose | 40.7 ± 1.0 | 4.4 ± 0.2 | 12.0 ± 0.6 | 14.5 ± 0.9 | 55.2 ± 1.9 |
| NMMO cellulose | 40.9 ± 0.9 | 1.3 ± 0.1 | 20.2 ± 0.2 | 10.3 ± 1.3 | 51.2 ± 1.4 |
| Langmuir-Schaefer cellulose | 42.4 ± 0.9 | 2.0 ± 0.1 | 9.6 ± 0.5 | 8.8 ± 1.0 | 51.2 ± 1.9 |

The calculated values in Table 2 indicate that the dispersive part of the cellulose surface energy is larger than the polar contribution, because the surface energy of cellulose determined by contact angle measurements is known to be ca. 55 $mJ/m^2$.[108] Kontturi et al. reported a surface energy of nanocrystal cellulose films as high as 65 $mJ/m^2$.[61] Reported values for the dispersive part of the surface energy of NMMO cellulose films are 40 and 44 $mJ/m^2$, determined by contact angle measurements.[108, 123] These values are similar to the values obtained in the present study. Table 2 also shows that the cellulose films exhibit basic surface characteristics, which might be somewhat unexpected since the cellulose surfaces, at least these of HC-MFC and nanocrystals, should have numerous acidic groups. On the other hand, a basic nature of fibrils/fibers is not surprising, since the Van Oss method[107] frequently used to determine these properties, often results in surfaces with basic properties.[124-126] The difference in total surface energy of the cellulose films, as obtained from contact angle measurements, is small. It is therefore difficult to draw conclusions regarding the influence of crystallinty and structure on the surface energy of the cellulose films.

Earlier surface energy determinations are summarized in Table 3. The results show that there is a large scatter in the data, especially for the polar components. This is probably due to both the nature of the cellulosic material and the method used for characterisation.

***Table 3.*** *Literature values of the surface energy of various cellulosic materials.*

| | Dispersive component ($mNm/m^2$) | Polar component ($mNm/m^2$) | Total surface energy ($mNm/m^2$) |
|---|---|---|---|
| Cellulosic material: | | | |
| Nanocrystal cellulose[51] | 42 | | |
| NMMO cellulose[51] | 40 | | |
| LiCl/DMAc cellulose[51] | 41 | | |
| Nanocrystal cellulose[61] | 32 | 33 | 65 |
| Cellulose acetate[108] | 44.9 | 8.7 | 53.6 |
| Cellulose acetate[127] | 39.1 | 17.8 | 56.9 |
| NMMO cellulose[123] | 40 | | |

The molecular structures of the cellulose films were resolved by small incidence angle X-ray diffraction and the results clearly show that the cellulose molecular structure and degree of crystalline ordering of the films depend on the choice of dissolving process. Table 4 summarizes the apparent crystallinity and the crystallite sizes of the cellulose model films obtained using the Scherrer equation.[128] The crystallinity values from a SPring-8 X-ray diffraction apparatus agree with those obtained using a laboratory apparatus within the experimental error.

***Table 4.*** *Apparent crystallinity and crystallite size of the cellulose model films.*

| | Crystallinity (%) | | Crystallite size (nm) | | |
|---|---|---|---|---|---|
| | SPring-8 | Laboratory | SPring-8 | | |
| Cellulose I crystal structure: | | | $1\bar{1}0$[a)] | 110[a)] | 200[a)] |
| LC-MFC 1 layer | 70.0 | 66.5 | 2.7 | 5.2 | 2.7 |
| LC-MFC 6 layers | | 60.5 | | | |
| PEI/HC-MFC 1 bilayer | | 64.5 | | | |
| PEI/HC-MFC 7 bilayers | 62.0 | 54.4 | 2.1 | 4.1 | 3.0 |
| Nanocrystal | 87.0 | 85.1 | 3.2 | 6.9 | 3.5 |
| Cellulose II crystal structure: | | | | | |
| NMMO | 58.0 | 60.0 | 2.8 | 2.0 | 2.3 |
| LS | 63.0 | 53.5 | 2.9 | 2.1 | 3.0 |
| LiCl/DMAc | | 14.8 | | | |

a) Based on cellulose Iβ

From these XRD studies (table 4) it was found that the cellulose film from LiCl/DMAc almost totally lacks crystalline order (14.7%), which indicates that the dissolving chemicals in this case penetrate or destroy the domains in the native cellulose. The NMMO and LS cellulose films clearly exhibited cellulose II structures and a significantly higher degree of crystalline order than the LiCl/DMAc cellulose II films. The NMMO film thus re-crystallizes during or after the dissolving process in NMMO. More open fibrillar network films have also been created by treating the substrates with dispersions of LC-MFC, HC-MFC or nanocrystals, using a spin-coating or dipping technique. The XRD analysis shows that the

more open fibrillar films were composed solely of cellulose I and indicate that the degree of crystallinity of the LC/HC-MFC and nanocrystal remains intact after the preparation of these films. The degree of crystalline order is, as expected, higher for the nanocrystal films than for the MFC films, since the hydrolysis step during the preparation degrades only the amorphous zones and not the crystalline zones of the native microfibrils.

### 4.1.2 The formation of multilayer films incorporating microfibrillated cellulose

Polyelectrolyte adsorption and particularly the polyelectrolyte multilayer (PEM) technique have proven to be useful tools for modifying the properties of different surfaces.[129] In papers I - IV, the LbL technique has been shown to be a useful tool for the build-up of cellulose model films. It is valuable to study in more detail how each polyelectrolyte/colloid is adsorbed in order to obtain better control of the build-up process. In paper II, the build-up of PEI/anionic MFC films was studied *in situ* using the DPI and QCM-D techniques, and each new adsorbed layer resulted in a clear change in total layer thickness and refractive index (as monitored by DPI), and in frequency and dissipation (as monitored by QCM-D). MFC multilayer films were formed using PEI as the cationic polyelectrolyte. PEI is commonly used as the cationic polyelectrolyte in PEM:s, especially as pre-cursor layer, due to its high charge density and ability to strongly adhere to most surfaces.[62, 90, 130] All the experiments were conducted using 100 mg/l PEI at pH 10 and 100 mg/l anionic MFC at pH 6.5. Overall, the general trends were basically similar for the studied systems, exhibiting a reproducible multilayer build-up in terms of adsorption kinetics and adsorbed amount of the individual layers, as shown in figure 14a and c. The results obtained by DPI show that there are differences in the growth of the multilayer thickness depending on the polyelectrolyte/colloid that is used. A larger increase in thickness is associated with the adsorption of MFC compared with the increase associated with the adsorption of PEI. For the MFC, the increase in thickness is smaller for the first two layers and then reaches a steady build-up with a larger increase in thickness for the MFC layers and a much smaller layer increase for the PEI layers. A total thickness of around 30 nm was obtained for five PEI/anionic MFC bilayers.
The change in refractive index as a function of layer number of PEI and MFC is shown in figure 14b. An increase in the number of PEI/anionic MFC layers is associated with an overall decrease in refractive index. The decrease in refractive index during multilayer build-up indicates that the average density of the layers decreases, which can be interpreted as indicating a more open structure of the multilayer created by the stiff microfibrils. The average refractive index of five bilayers was approximately 1.48.

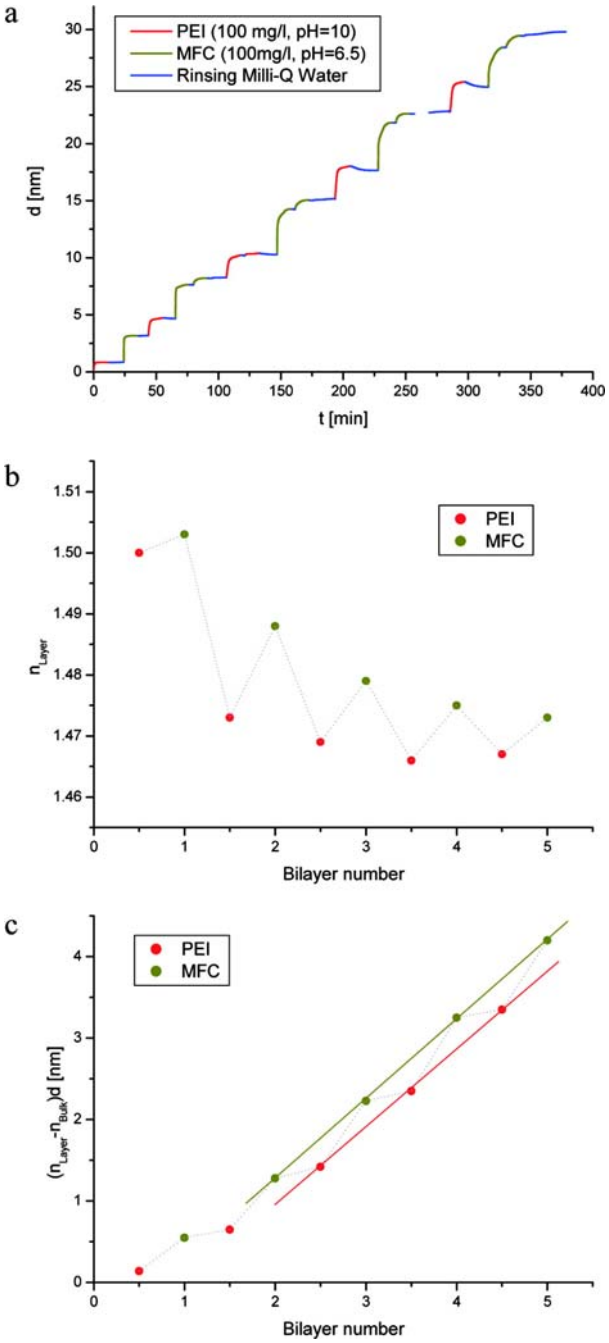


*Figure 14. (a) Kinetics of adsorption and calculated total thickness, d, (b) refractive index, n, and (c) an entity proportional to the adsorbed amount* ($(n_{layer} - n_{bulk}) \times d$ *(nm)) for the individual layers as a function of bilayer number for multilayer formation of PEI/anionic MFC on the silicon oxynitride surfaces determined by DPI. The PEI concentration was 100 mg/L at pH 10, and the MFC concentration was 100 mg/L at pH 6.5.*

From QCM-D measurements, the viscoelastic properties of the multilayer formed were examined by studying the changes in energy dissipation (figure 15a). When the multilayer formation was carried out, there was a large increase in dissipation associated with the adsorption of the MFC layers, which indicates a more open and thicker structure compared to the PEI layers. The large increases in dissipation matches well with the decrease in average refractive index measured by DPI (figure 14b), indicating that the average surface density of the layers decreases with increasing layer number.

Additional information was obtained about the mass-uptake as a decrease in frequency of the 3rd, 5th and 7th overtones as shown in figure 15b. The adsorption kinetics of the individual layers was similar to that measured with DPI (figure 14a). The adsorption phases could be distinguished as follows: a rapid and smaller adsorption associated with PEI followed by a slower and larger adsorption associated with the injection of MFC. The adsorption kinetics became slower for each new layer of MFC adsorbed, possibly, due to a re-configuration or self-organisation of the microfibrils on the surface.

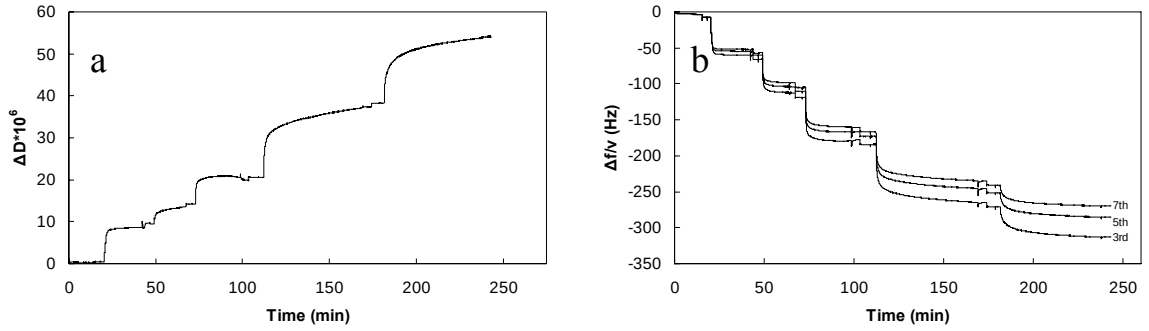


*Figure 15. (a) QCM-D data showing the change in energy dissipation as a function of the adsorption and build-up of multilayers of PEI and anionic MFC. The PEI concentration was 100 mg/l at pH 10 and MFC concentration was 100 mg/l at pH 6.5. This data is from the third overtone (15 MHz). (b) QCM-D data showing the change in normalized frequency as a function of the overtone.*

The DPI and QCM-D data have so far been presented in their original form, but it is also interesting to interpret the data in terms of adsorbed amounts. The previously described de Feijter[131] and Sauerbrey[132] equations were applied to estimate the adsorbed amount from the DPI and QCM-D measurements, respectively. The adsorbed mass of the five-bilayer multilayer was estimated from DPI and QCM-D measurements to be 32.6 mg/m$^2$ and 55.4 mg/m$^2$, respectively. The calculations indicate that the solvent contributed a large part, i.e. ca. 41%, of the adsorbed mass. This may be due to mechanically trapped water in the pores among the MFC fibers, significant hydration of the carboxymethylated microfibrils and/or associated water of the PEI.

### 4.1.3 Multilayer formation of PEI/anionic MFC and cationic MFC/anionic MFC – a comparison

As most polyelectrolytes used for multilayer build-up are petroleum-based, MFC, a biorenewable cellulose derivate, would be of interest and an ideal candidate as a base for bio-based multilayers.
In paper IV, SPAR was used to study the multilayer formation of cationic MFC/anionic MFC and PEI/anionic MFC. The results are presented as the relative change in the reflected signal ($\Delta S/S_0$) and thereby used to monitor the formation of the multilayer. Following each MFC treatment, a rinsing step was performed with Milli-Q water. The multilayer growth was linear and equilibrium was reached quite rapidly (figure 16a). These results indicate that such large and semi-crystalline polyelectrolytes/colloids with low-charge density (D.S. ≈ 0.1) also have the ability to form multilayers. When PEI and anionic MFC were used (figure 16b), a much larger increase in the detected signals was observed, particularly those associated with the adsorption of MFC.

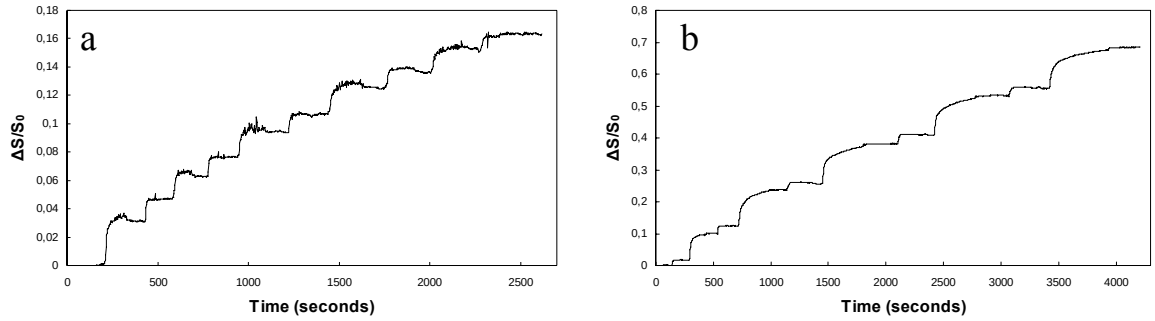


*Figure 16. SPAR data showing the relative change in the detected signal as a function of the adsorption and build-up of a) cationic MFC/anionic MFC and b) PEI/anionic MFC multilayers. The build-up was performed using PEI and cationic/anionic MFC dispersions with concentrations of 100 mg/l. Rinsing with Milli-Q water was performed after each adsorption step.*

The adsorbed mass and viscoelastic properties of the formed multilayers were obtained from QCM-D measurements. The highly swollen multilayer films formed by the adsorption of the more open, less rigid and bulky MFC, were highly viscoelastic. This is indicated by the high dissipation values accompanying the adsorption of MFC as shown in figure 17a and b. The dissipation values may also be a result of the MFC fibrils oriented outwards into the solution. The higher adsorbed mass of the PEI/anionic MFC (figure 17d) than of the cationic MFC/anionic MFC multilayer (figure 17c) may be a consequence of the difference in flexibility and geometrical restriction of the PEI molecules and MFC fibrils. PEI is a highly charged and branched molecule known to form almost sphere-like structures in water[89, 90, 130, 133, 134] and being able to penetrate into the voids of the highly swollen MFC fibril network. Due to the relatively high charge of the PEI, this polyelectrolyte may also completely over-charge the oppositely charged silicon or MFC surface. Since the charge of the MFC is much lower than PEI, the fibrils will adsorb in higher amount to compensate for the over-charged PEI surface. The excellent anchoring feature of PEI was previously found by Wågberg et al.[62] who studied the multilayer build-up of various cationic polyelectrolytes and anionic MFC using ellipsometry.

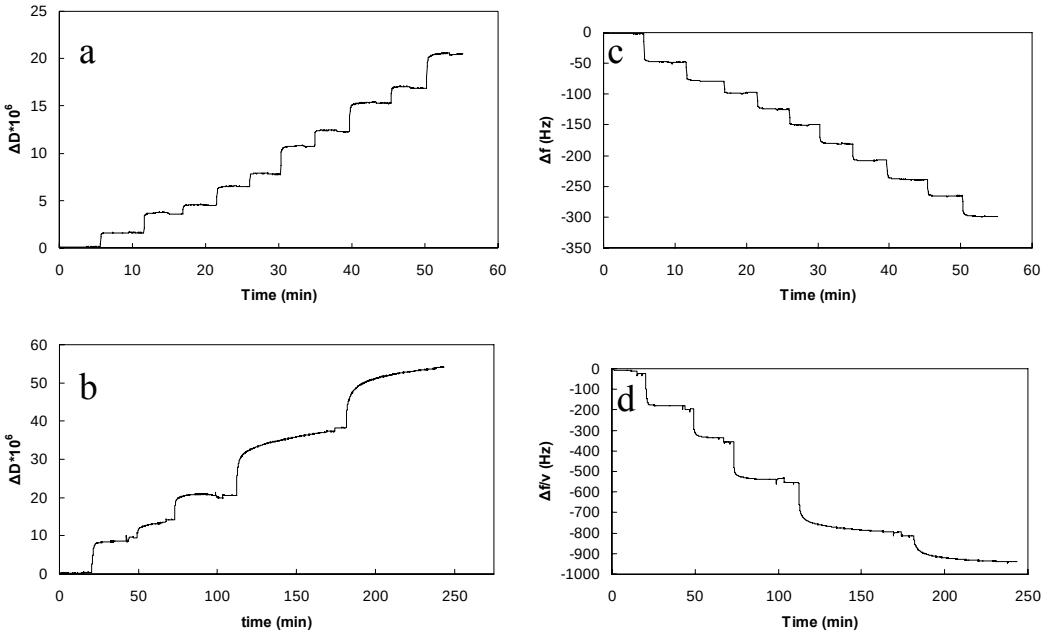


*Figure 17. Change in frequency (from the third overtone), Δf, and energy dissipation, ΔD, as a function of the build-up of multilayers of (a, c) cationic MFC/anionic MFC and (b, d) PEI/anionic MFC.*

AFM height and phase images of a five-bilayer cationic/anionic MFC multilayer film show a fibrillar network (figure 18a and b). The microfibrils appear, as expected, as stiff rods. Taking into consideration the broadening due to the geometry of the tip, direct measurement of the fibrils in figure 18 shows an average width of 4 nm. AFM images of a five-bilayer PEI/anionic MFC surface are also shown in figure 18c and d. The microfibrils fully cover the silica surface. This indicates, as previously discussed, that PEI functions as an effective anchoring polyelectrolyte between the geometrically restricted MFC fibrils. It is interesting to note that the differences in frequency changes and detected signals for the multilayer films (PEI/anionic MFC > cationic MFC/anionic MFC) as monitored by SPAR and QCM-D, respectively, well match the AFM images, clearly demonstrate the differences in surface coverage of the fibrils.

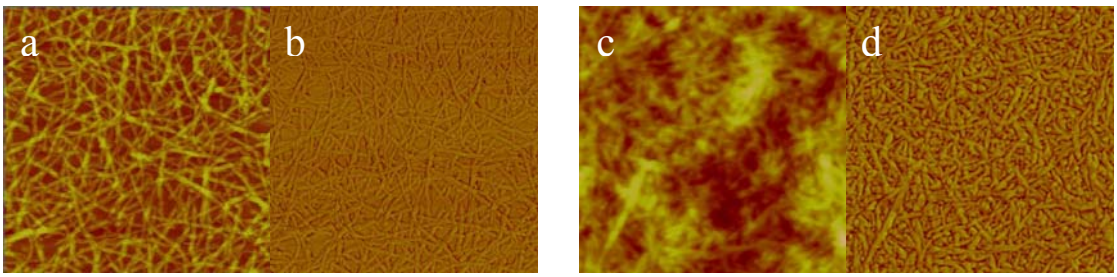


*Figure 18. AFM height and phase images of the five-bilayer multilayer films on silica. (a) Height and (b) phase images of cationic/anionic MFC and (c) height and (d) phase images of PEI/anionic MFC. The scanned surface areas were 1 μm$^2$.*

## 4.2 Design of structured cellulose surfaces (papers VI and VII)

### 4.2.1 The formation of structured multilayer films incorporating cellulose nanocrystals

Figure 19 shows representative top (left column) and tilted (20º) (right column) FE-SEM micrographs of structured silicon surfaces prepared by a plasma etching process (paper VI). Polished silicon wafers were thermally oxidized and patterned in an array of circles with a diameter of 1-2 μm and with a peak-to-peak distance of 2-4 μm using standard photolithography followed by anisotropic plasma etching. The plasma etching was performed by the Bosch process in a STS Multiplex ICP (Inductively Coupled Plasma Etching) system.[135] The etching and passivation gases were $SF_6$ and $C_4F_8$, respectively. The wafers were etched for 40, 30, 20 and 10 min and are referred to as surfaces A - D, respectively. The structured silicon surfaces were treated with five bilayers of PEI and cellulose nanocrystals, and are hereafter referred to as cellulose surfaces A - D.

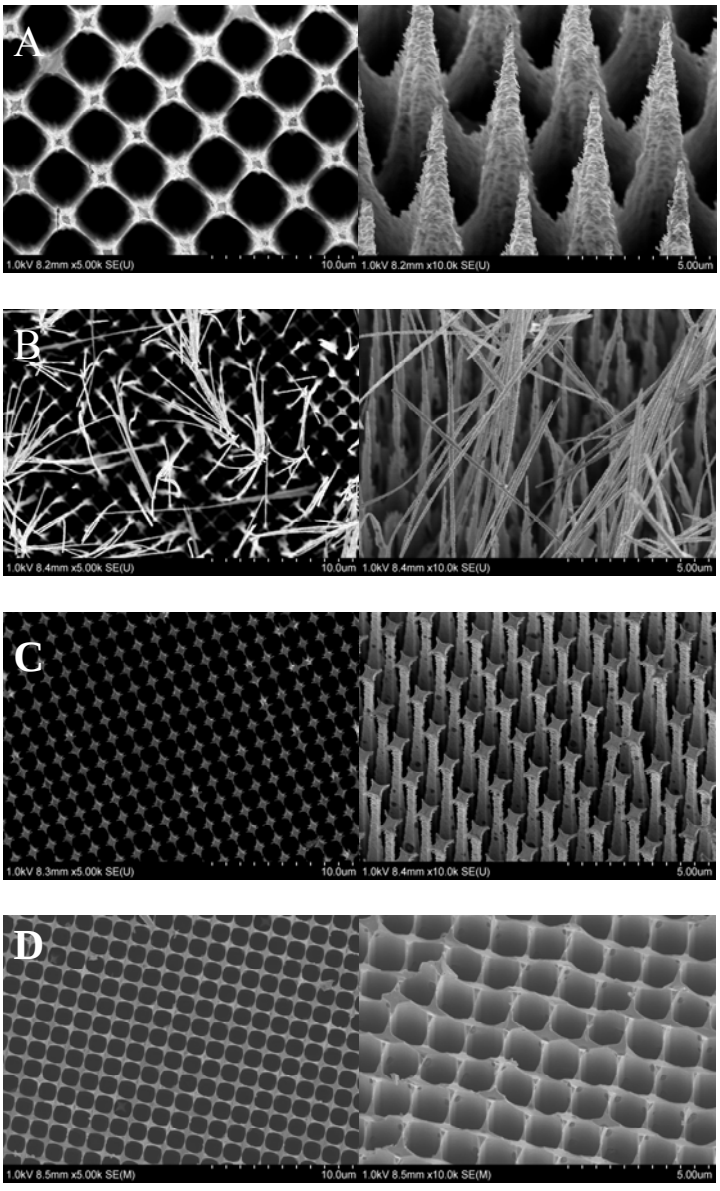


*Figure 19. FE-SEM micrographs of porous silicon surfaces fabricated by plasma etching. The surfaces are referred to as A - D (from above). The left column shows top-view images*

*(magnification x5000) and right column images obtained at a tilt angle of 20º (magnification x10000).*

Figure 20 present a FE-SEM micrograph of a planar cellulose nanocrystal film at a magnification of x60000. The cellulose nanocrystals were successfully incorporated into a multilayer film containing PEI and adsorbed onto the planar silicon surface. The random orientation and distribution of the nanocrystals is apparent in the micrograph. Cellulose nanocrystals were estimated to have dimensions of ca. 10 nm by 200 nm.

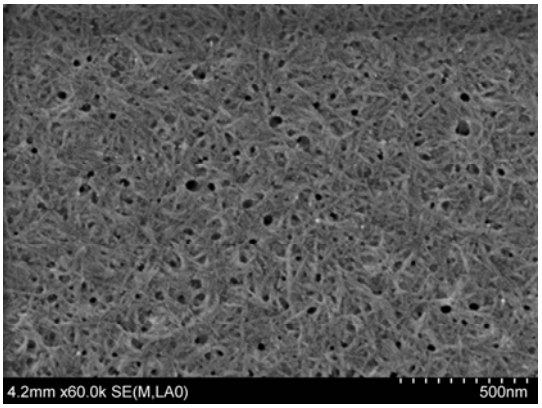


*Figure 20. FE-SEM micrograph (x60000) of a multilayered film of PEI and cellulose nanocrystals (5 bilayers) prepared by solution-dipping of a planar silicon surface.*

Figure 21 shows FE-SEM micrographs of a structured silicon surface (surface B, see figure 19b) and the same surface treated with five bilayers of PEI and cellulose nanocrystals. The FE-SEM micrographs indicate that the structured silicon surface is covered with layers of cellulose and that the coated silicon pillars/wires are rougher and broader than the uncoated ones. A “film-like” structure is apparent on the nanowires.

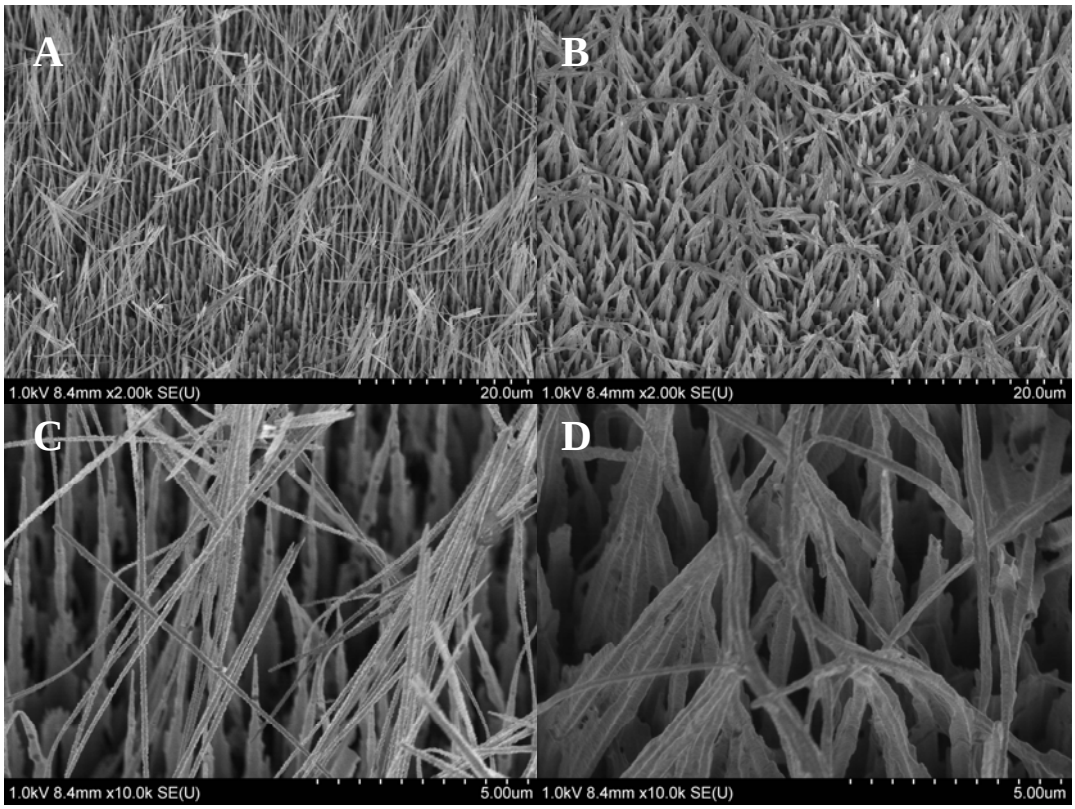


*Figure 21. FE-SEM micrographs at magnifications of x2000 and x10000 of (b, d) multilayered films of PEI and cellulose nanocrystals (5 bilayers) and their (a, c) silicon analogues.*

XPS measurements strongly support the cellulose modification of the structured and flat silicon surface. Survey spectra of the cellulose films showed carbon, oxygen and small amounts of nitrogen and sulphur on the surface. No silicon was detected. The trace amounts of sulphur are due to sulphate ester groups resulting from hydrolysis with sulphuric acid during preparation of the cellulose nanocrystals. Taking into account the fact that the depth of analysis by XPS is about 10 nm, this indicates a dense film characteristic thickness of > 10 nm.

### 4.2.2 Microfibrillated cellulose aerogels with different surface textures

Figure 22 show FE-SEM micrographs of the surface of MFC aerogels with densities of 0.00027, 0.0018, 0.0053, 0.0070, 0.011 and 0.030 g/cm$^3$. The aerogels were prepared by freeze-drying MFC dispersions with concentrations of 0.0031% to 3.13%. As expected, an increase in MFC dispersion concentration resulted in an aerogel with a higher density. The densities of the aerogels are very low, less than 0.03 g/cm$^3$, which means that they have a very high porosity. As seen in figure 22, an increase in aerogel density results in a greater closure of the surface texture, with fewer pores on the surface. The surface appears smoother for aerogels with higher density ($\rho \approx 0.03$ g/cm$^3$) (figure 22f). Aerogels with lower density ($\rho <$ 0.0070 g/cm$^3$) (figure 22a, b and c) reveal a more open surface with sheets of MFC protruding out from the surface. In addition, microfibril bundles protruding out from the surface are forming loosely interconnected networks. The surface texture can thus be tuned by changing the concentration of the MFC dispersion before freeze-drying.

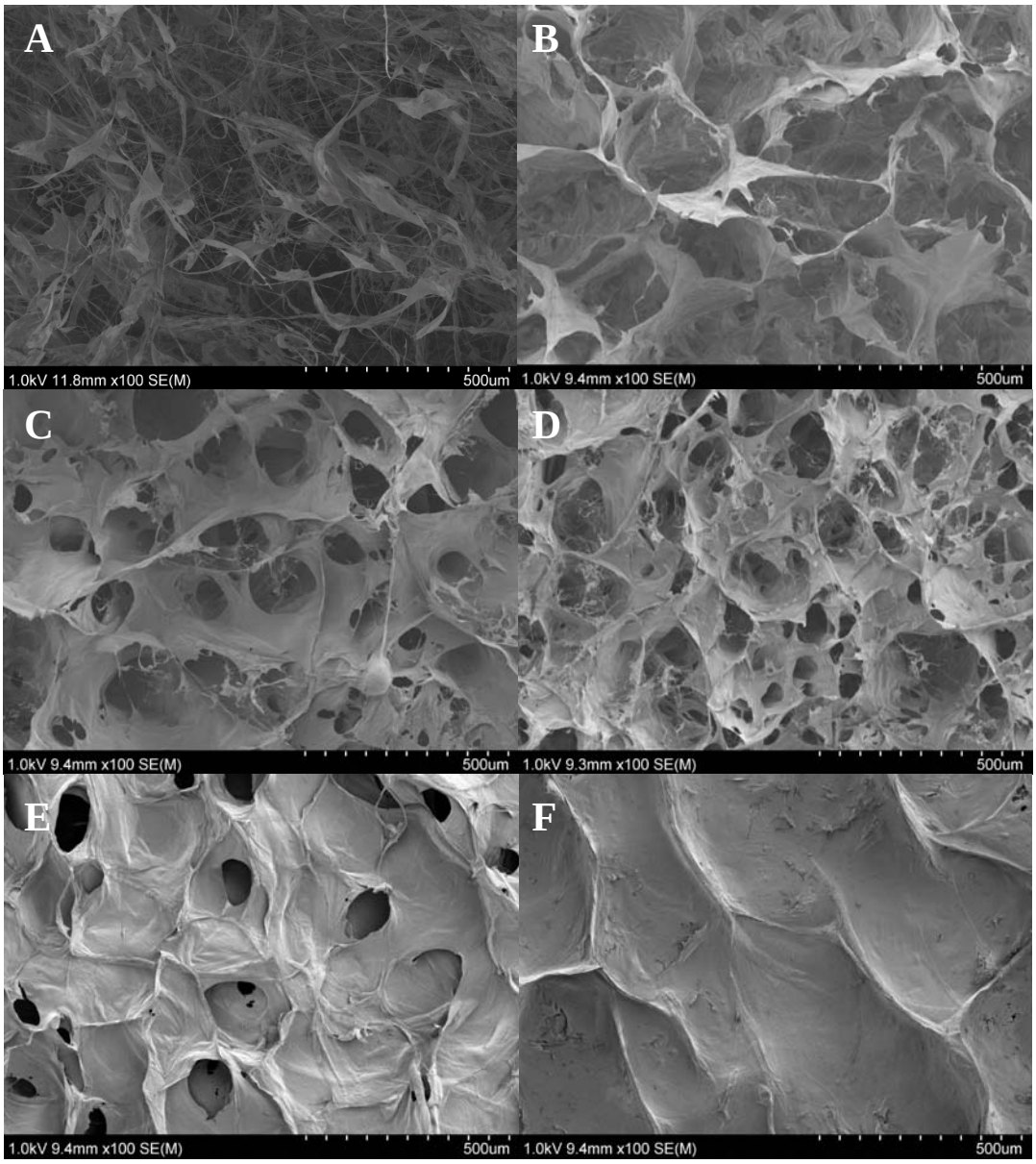


*Figure 22. FE-SEM micrographs of aerogels fabricated by freeze-drying aqueous MFC dispersions. The densities of the aerogels are (a) 0.00027 (b) 0.0018 (c) 0.0053 (d) 0.0070 (e) 0.011 and (f) 0.030 g/cm$^3$ All images are top-view images and the scale bars are 500 µm.*

## 4.3 Adsorption of fluorinated compounds on cellulose surfaces (papers I, VI and VII)

In order to prepare cellulose surfaces with oleophobic properties suitable for wetting studies by low surface energy oil mixtures and alkanes, the substrates were treated with variuos fluorinated compounds; fluorosurfactants, fluorinated silanes or pentadecafluorooctanyl chloride.

### 4.3.1 Perfluorooctadecanoic acid in solution and adsorbed on cellulose surfaces

A fluorinated surfactant, perfluorooctadecanoic acid, was adsorbed onto the regenerated NMMO cellulose II and PEI/HC-MFC surfaces (paper I). Here, only the adsorption onto the NMMO cellulose surfaces will be discussed. The adsorption of a fluorosurfactant onto a cellulose surface depends on several factors. Probably, one of the most important is the structure of the surfactant, including its length. A cationic fluorosurfactant, $CF_3(CF_2)_nSO_2NH(CH_2)_3$-$4N(CH_3)_3^+I^-$, and perfluorooctaoic acid were found to be desorbed from the cellulose surfaces upon rinsing with Milli-Q water, whereas a dispersion of perfluorooctadecanoic acid was completely attached to the surface and resisted rinsing. This latter driving force for perfluorooctadecanoic acid is related to the surfactant structure and length, which also affect its solubility characteristics in water.
The aggregation of perfluorooctadecanoic acid at a concentration of 100 mg/l in aqueous solution has here been studied using Cryo-transmission electron microscopy (Cryo-TEM). The experiments indicated that self-assembly of the surfactant into large polydisperse micelle structures in the range of 50 to 500 nm occurred (figure 23). As perfluorooctadecanoic acid is very hydrophobic in nature, exhibiting low solubility in water as indicated by Cryo-TEM, a rather large hydrophobic driving force for adsorption is expected, and this surfactant dispersion was, hence, found suitable for modifying the cellulose surfaces.

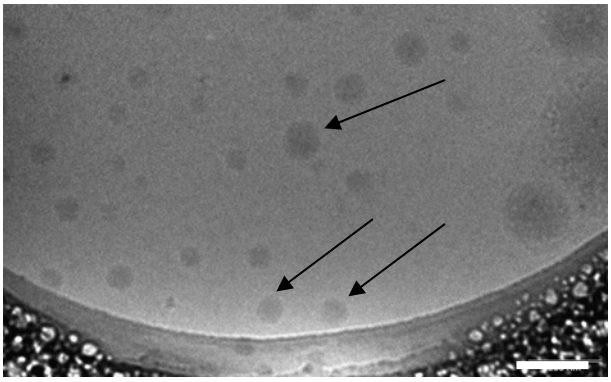

*Figure 23. Cryo-TEM micrograph of micelles, indicated by arrows, formed in an aqueous solution of 100 mg/l perfluorooctadecanoic acid at pH 7. Scale bar = 200 nm.*

Figure 24 shows the influence of the perfluorooctadecanoic acid concentration after 20 min adsorption on the atomic surface fluorine concentration on the NMMO cellulose II films as measured by XPS. As the perfluorooctadecanoic acid concentration increased, the surface concentration of fluorine increased until a saturation plateau was reached at approximately 150 mg/l. As the concentration of surfactant solution increased, the amount of surfactant coating increased to ca. 60 atomic % at a concentration of 150 mg/l. The fluorine concentration of pure perfluorooctadecanoic acid was determined by XPS to be approximately 64%. It is therefore believed that, in the case of 60 at.% fluorine concentration, the XPS is detecting almost pure perfluorooctadecanoic acid on the surface. A rather thick bilayer (> 10 nm) of coated perfluorooctadecanoic acid is probably formed, since the depth of the XPS analysis is of the order of 10 nm.

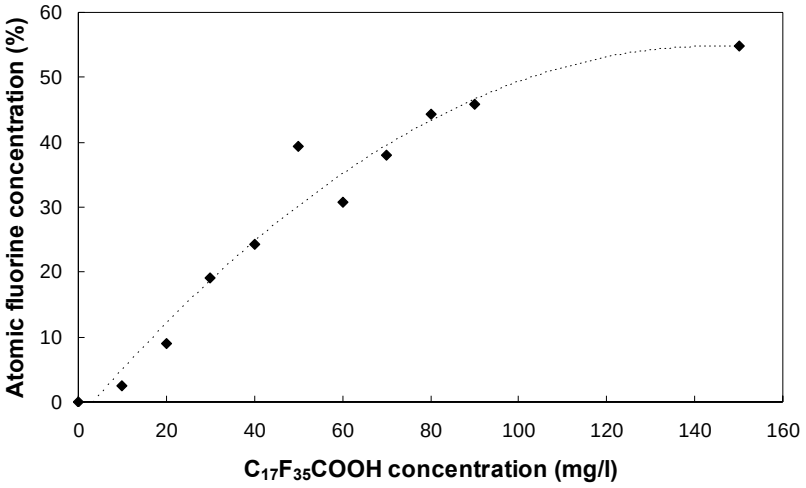


*Figure 24. Atomic surface fluorine concentration on regenerated cellulose II surfaces as a function of fluorosurfactant concentration during adsorption (20 min).*

In order to determine the dispersive surface energy of the regenerated cellulose surfaces, contact angles were measured with methylene iodide and n-hexadecane. The calculations were according to:[107, 108]

$$2\sqrt{\gamma_s^d \gamma_l^d} = \gamma_l(1+\cos\theta_e) \qquad (11)$$

where $\gamma_s^d$ is the dispersive surface energy of the cellulose surface, $\gamma_l^d$ the dispersive surface tension of the liquid, $\gamma_l$ the surface tension of the liquid and $\theta_e$ the equilibrium contact angle between the liquid and the cellulose surface. Equation 11 is valid when the interactions between the liquid and the surface are totally dominated by dispersive interactions.[107, 108] Figure 25 shows the calculated dispersive surface energy vs. atomic fluorine concentration for the NMMO cellulose II surfaces. At zero surfactant concentration, i.e. on pure regenerated cellulose surface, the dispersive surface energy was 45.1 mN/m. When the surface concentration of fluorine was increased slightly, the dispersive surface energy decreased drastically. A further increase in the atomic fluorine concentration led to a further decrease in the dispersive surface energy until saturation was reached at a dispersive surface energy of about 12 mN/m. Figure 25 can be interpreted as indicating that the surfactant coverage on the regenerated cellulose is incomplete at very low surface concentration of fluorine as the fluorosurfactant molecules are probably lying flat on the surface. As the fluorine concentration increases, there is a decrease in dispersive surface energy probably due to a reorientation of the surfactant molecules from a flat, via an intermediate position, to a position where the fluorocarbon tails are oriented more or less perpendicular to the surface. A further increase in atomic concentration of fluorine may lead to the formation of multiple surfactant layers, and the measured dispersive surface energy levels off and is then constant at higher fluorine concentrations (> 45 at.%).

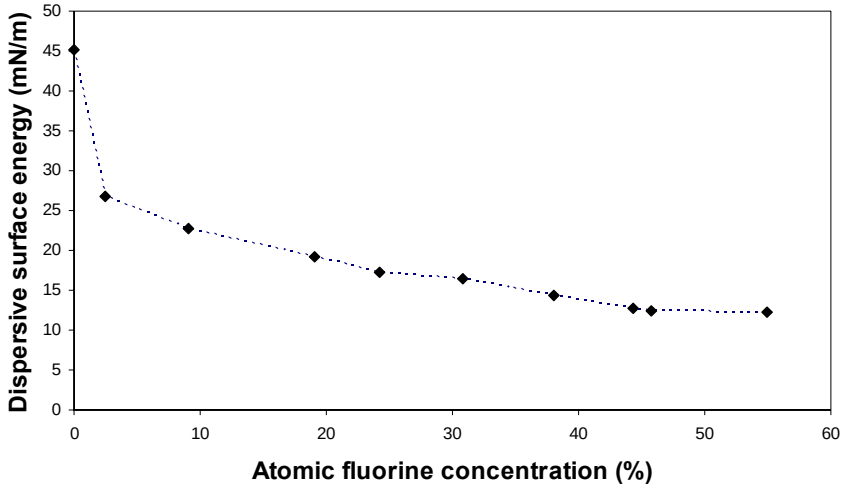


*Figure 25. Dispersive surface energy of fluorinated regenerated cellulose II surfaces as a function of the atomic fluorine concentration.*

For the regenerated cellulose surfaces with the highest surfactant concentration, the dispersive surface energy was determined to be about 12 mN/m. Amongst the numerous molecular structures investigated, a close-packed uniform $CF_3$ surface had the lowest surface tension (6 mN/m).[136] The critical surface tension for $CF_2$-$CF_2$ groups was determined by Zisman et al. to be 18 mN/m,[137] which indicates that the surfactant-coated surfaces are enriched by $CF_3$ groups.

### 4.3.2 Pentadecafluorooctanoyl chloride-modification of cellulose surfaces

The hydroxyl groups on the NMMO cellulose surfaces were modified with pentadecafluorooctanyl chloride (paper I). XPS analysis confirmed the success of the acylation reaction. For the covalently modified regenerated cellulose II films, the atomic fluorine concentration was fairly constant with varying concentration of pentadecafluorooctanyl chloride in the reaction mixture (table 5). It can thus be assumed that a monolayer of pentadecafluorooctanyl chloride covalently bonded to the regenerated cellulose surface has been formed. The dispersive surface energy of the covalently modified cellulose films was determined to be 12.5 mN/m.

***Table 5**. Atomic surface concentrations on NMMO cellulose films covalently modified with varying concentration of pentadecafluorooctanyl chloride.*

| | Surface concentration (atomic %) | | |
|---|---|---|---|
| | C | O | F |
| 50 µl | 37.57 | 7.87 | 54.55 |
| 200 µl | 35.92 | 8.07 | 56.00 |
| 400 µl | 35.60 | 7.98 | 56.42 |

### 4.3.3 Fluorinated silanes on structured cellulose surfaces

A fluorinated trichlorosilane-coating (PFOTS-coating) process was applied to structured cellulose surfaces with reactive OH-groups derived from the cellulose nanocrystals (paper VI)

or HC-MFC cellulose aerogels and films (paper VII). The unique surface texture of the cellulose substrates and the PFOTS-coating were found to significantly decrease the wetting properties of various non-polar liquids as will be discussed later.
XPS measurements strongly support the successful chemical modification of the nanocrystal cellulose surfaces. A summary of the atomic concentrations for pure and PFOTS-coated planar and structured cellulose nanocrystal surfaces is given in Table 6. XPS detected carbon, oxygen and small amounts of nitrogen and sulphur on the pure cellulose surface. The amount of fluorine on the PFOTS-coated cellulose surface after the coating was found to be ca. 31-34%

***Table 6.*** *Atomic surface concentration on PFOTS-coated and non-coated structured and planar cellulose surfaces.*

| | Surface concentration (at.%) | | | | | |
|---|---|---|---|---|---|---|
| | C | O | N | S | Si | F |
| Cellulose nanocrystal surfaces | 60 | 38 | 2 | 1 | | |
| Planar PFOTS-coated silicon surfaces | 46 | 20 | 1 | | 2 | 31 |
| Structured PFOTS-coated silicon surfaces | 45 | 18 | 1 | | 2 | 34 |

The atomic fluorine and carbon concentrations of a pure fluorinated trichlorosilane compound were determined by XPS to be approximately 53 and 37%, respectively. Since the depth of the XPS analysis is of the order of 10 nm, and a significant amount of carbon (ca. 45-46%) was detected by the XPS in the PFOTS-coated cellulose surfaces, it is believed that the fluorinated trichlorosilane is adsorbed as a very thin film (< 10 nm).
The high concentration of fluorine, as indicated by the XPS analysis, results in very oleophobic materials with low surface energy. The dispersive surface energy of the flat cellulose surface was determined to be 15 mN/m by contact angle measurements according to equation 11,[107, 108] using hexadecane as probe liquid.
As previously discussed, a $CF_3$ surface had the lowest surface free energy measured (ca. 6.7 mN/m).[136] Taking this into consideration, these studies can explain why hexadecane and decane displayed contact angles < 90º against the flat cellulose surface since these surfaces would need surface energies of ca. 6.9 and 6.0 mN/m, respectively, for these liquids to have a contact angle $\theta > 90º$.
The surface chemistry of the HC-MFC aerogels and films was controlled by the chemical vapour deposition (CVD) of fluorinated trichlorosilane. As with the fluorinated cellulose nanocrystal surfaces, the HC-MFC aerogels and films had a very high atomic fluorine concentration after modification. XPS measurements detected ca. 51% fluorine on the MFC surfaces.

## 4.4 Wetting of oil mixtures and alkanes on fluorinated cellulose surfaces (papers I, VI and VII)

### 4.4.1 Wetting by oil mixtures of smooth cellulose surfaces with different degrees of oleophobicity

The adsorption of fluorocompounds on cellulose has been shown to improve its repulsion of low surface tension components such as oils. To clarify the importance of the dispersive surface energy and the atomic fluorine concentration in the cellulose surface, the NMMO cellulose surfaces were coated for 20 min with different concentrations of perfluorooctadecanoic acid, ranging from 10 to 150 mg/l. Figure 26 shows the spreading of castor oil on a pure cellulose surface and on cellulose models coated with different amounts of

adsorbed fluorosurfactant. A logarithmic time scale has been chosen. This figure shows that there is a large difference in the spreading kinetics of castor oil between fluorinated cellulose surfaces and an uncoated pure cellulose surface. The contact angle is larger and the approach to a constant contact angle is much more rapid with increasing concentration of perfluorooctadecanoic acid. The contact angle remained the same for substrates treated with surfactant concentrations of 50 mg/l and above.

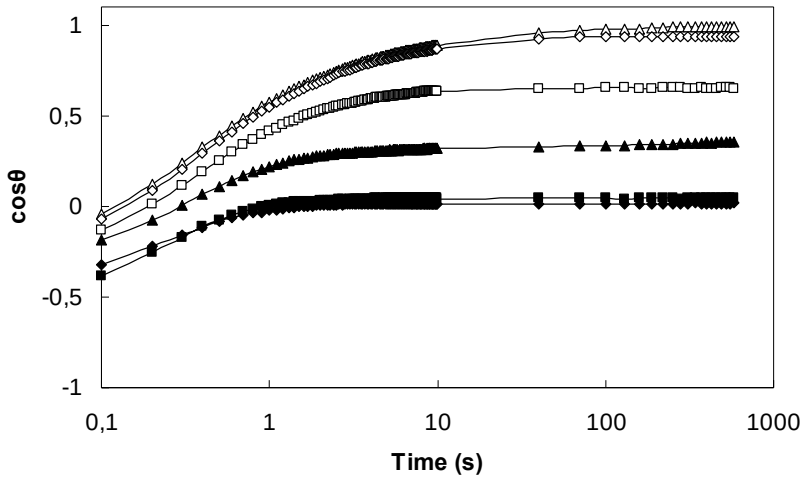


*Figure 26. Cosθ vs. time for castor oil on PEI pre-treated cellulose model surfaces coated with different amounts of adsorbed fluorosurfactant. (Δ) 0 mg/l (uncoated, pure cellulose surface), (◊) 10 mg/l, (□) 20 mg/l, (▲) 30 mg/l, (♦) 40 mg/l and (■) 50 mg/l.*

Figure 27 shows cosθ plotted versus the contact time for oil mixtures 1, 3 and 6 on perfluorooctanoyl chloride-modified and pure NMMO cellulose surfaces. In the case of kit mixtures 1 and 3 on perfluorooctanoyl chloride-modified cellulose surfaces, the spreading process can be subdivided into two stages. In both cases, the dynamic contact angle decreases very rapidly over the first stage of spreading until a constant value, $\theta_e$, is reached. The spreading rate in the first stage is greater for kit mixture 1 than for kit mixture 3 due to the greater driving force for spreading i.e. $\theta/\theta_e$. The dynamic contact angle remained constant, $\theta_e$, over most of the second stage and the mixtures were found to be non-wetting with $\theta_e > 90^o$. The spreading behaviour for kit mixture 6 was different from that of kit mixtures 1 and 3. No significant spreading regime was observed and no equilibrium state with constant θ was reached for kit mixture 6 during the time of the measurements. The dynamic contact angle evolution with time of the kit mixtures on a pure cellulose surface is also presented in figure 27. For all three oil mixtures, the spreading was continuous almost until $\cos\theta = 1$ is reached, and it is difficult to define any spreading regime exhibiting a distinct difference in velocity of spreading during the time of the experiments. The three curves almost condense to a single curve at the end of the time scale.

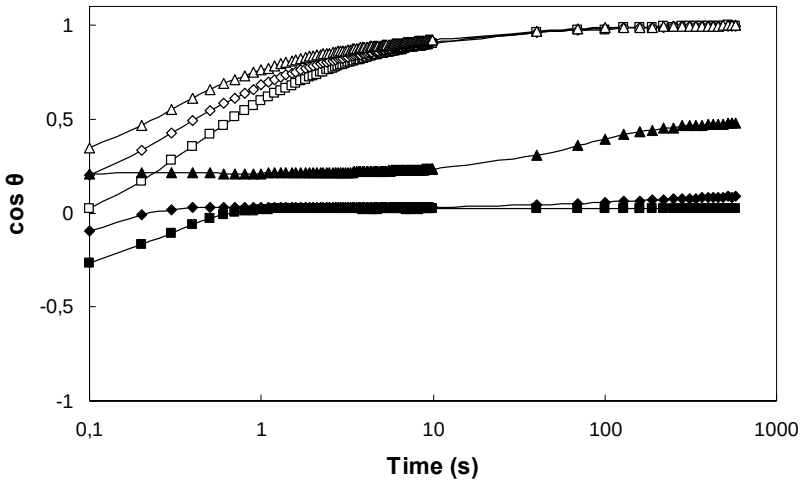


*Figure 27. (a) cosθ vs time for kit mixtures 1, 3 and 6 on perfluorooctanoyl chloride- modified and pure cellulose surfaces. Kit mixtures 1, 3 and 6 on perfluorooctanoyl chloride- modified cellulose surface: (■), (♦) and (▲), respectively. Kit mixtures 1, 3 and 6 on pure cellulose surface: (□), (◊) and (Δ), respectively.*

### 4.4.2 Wetting by castor oil and alkanes of structured cellulose surfaces

The wetting properties of structured and smooth cellulose nanocrystal surfaces were evaluated using castor oil, hexadecane and decane (table 7). The silicon analogues of the cellulose surfaces are shown in figure 19. The wetting properties of the cellulose surfaces are clearly influenced by the topography. Before PFOTS-coating, the cellulose surfaces were oleophilic with contact angles for castor oil, hexadecane and decane less than 5°. After the flat cellulose surface had been coated with a thin layer of PFOTS, the θ values of castor oil, hexadecane and decane on the PFOTS-coated cellulose were 72, 60, and 48°, respectively. When the coating was applied to structured cellulose films, they displayed highly oleophobic properties, with contact angles of 125 – 146° for castor oil (table 7).

***Table 7.*** *Contact angles for castor oil and alkanes on PFOTS-coated and non-coated structured and planar cellulose nanocrystal surfaces.*

| | Planar cellulose surfaces | Planar PFOTS-modified cellulose | PFOTS-modified cellulose surf. A. | PFOTS-modified cellulose surf. B. | PFOTS-modified cellulose surf. C. | PFOTS-modified cellulose surf. D. |
|---|---|---|---|---|---|---|
| $\theta_{\text{castor oil}}$ | <5º | 72º | 146º | 141º | 133º | 125º |
| $\theta_{\text{hexadecane}}$ | ~0º | 60º | 128º | 113º | 105º | 108º |
| $\theta_{\text{decane}}$ | ~0º | 48º | 107º | 98º | 79º | 88º |

Since the surface chemical composition was almost the same for the PFOTS-coated planar and structured cellulose (table 6), the structure-induced roughness is presumably the primary cause of the large difference in oleophobicity of these surfaces. Increases in oleophobicity due to rough or microstructured surfaces are often interpreted in terms of two possible models, originally described by Wenzel[68] and by Cassie and Baxter.[69] In the Wenzel state, the liquid is in contact with the entire solid surface and completely penetrates the gaps generated by the roughness. The effect of the surface roughness in this model is simply to increase the surface area. In contrast, the Cassie−Baxter model assumes that there is no penetration of liquid into

the gaps between the irregularities on the surface and that the liquid rests on the rough features of the protruding solid material. The air bridging these features then acts as a further support for the oil droplets, and apparent contact angle of the oil on the substrate is a composite effect of the interaction between the oil droplet and the solid and the oil droplet and air.

The key design feature of the structured cellulose surfaces in this study is that they possess both the desired characteristics of "roughness" ($r > 1$) and a low value for the wetted surface fraction ($f_1 < 1$) embodied in equations 2 and 3. As a consequence of the multiple scales of roughness and high porosity generated by the plasma etching process, the samples are expected to be best characterized by the Cassie-Baxter equation.

An important observation from table 7 is that the contact angles on the PFOTS-coated structured cellulose surfaces in most cases was > 90º, even though in each case the contact angle on the smooth surfaces was < 90º. This is surprising if it is assumed that for $\theta < 90°$, the rough surfaces are in the Wenzel state, so that from equation 2, $\theta^* < \theta$ is expected. This effect is further shown in the form of the general wetting diagram[71] in figure 28, which shows a plot of $\cos\theta^*$ on the rough PFOTS-coated cellulose surfaces as a function of $\cos\theta$ for the corresponding PFOTS-coated smooth surfaces. The surfaces display high apparent advancing contact angles ($\theta^*$) indicative of being best described by the Cassie-Baxter equation. Earlier experiments show that this Cassie-Baxter state is metastable; only locally stable, and that the energy barrier separating the Cassie-Baxter and Wenzel states are dependent on the topography of the surfaces under consideration.[78, 79, 138] However, figure 28 indicates a transition from the Wenzel state to the non-wetting Cassie-Baxter state at an equilibrium contact angle less than 90º.

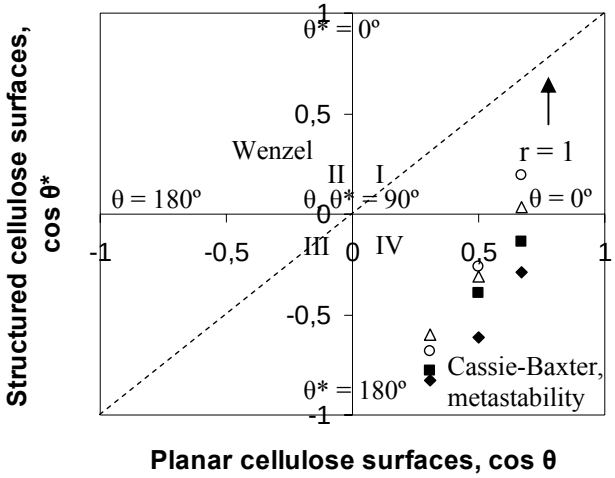


*Figure 28. Non-wetting diagram comparing the contact angles for various alkanes; castor oil, hexadecane and decane (left to right), on the structured and planar PFOTS-coated cellulose surfaces. Surface A, B, C and D: (♦), (■), (Δ) and (○), respectively. The surface texture generated by the plasma etching process allows the formation of a composite interface (Cassie-Baxter state) even with $\theta < 90º$. The surfaces in the lower right quadrant of this diagram correspond to oleophilic substrates that are rendered oleophobic purely by topography.*

Figure 29 shows the advancing contact angle for castor oil as a function of the density of the PFOTS-coated MFC aerogels. Comparing the aerogels with densities of 0.00035 and 0.00027 g/cm$^3$, there is a rapid transition from a perfectly non-wetting ($\theta >> 90º$) to a completely

wetting interface ($\theta \approx 0^{o}$). A contact angle denoted $\approx 0^{o}$ indicates that the surface was not sufficiently robust to support a 10 µl droplet of castor oil, and that the liquid droplet was imbibed into the surface.
The most oleophobic aerogel ($\rho = 0.0070$ g/cm$^3$) exhibited a contact angle of roughly 166° for castor oil which, to the knowledge of the authors, is among the highest contact angles found in the literature for this oil or liquids with similar surface tensions.[71, 74, 84, 139] As expected, there was a large difference between the contact angles on the structured aerogels and on the smooth solvent-casted MFC film. The contact angle for castor oil on PFOTS-modified MFC films was 96°. At densities higher than 0.020 g/cm$^3$, the contact angle gradually decreased with increasing density to a value in the vicinity of the contact angle of a smooth solvent-casted MFC film. This is probably due to the similar surface textures of the MFC aerogels at high-density (0.030 g/cm$^3$) and the solvent-casted MFC film. It is clear in figure 29 that, for very low-density aerogels (< 0.0003 g/cm$^3$), the liquid is in contact with the entire solid surface and completely penetrates the surface texture. The number of pores and the pore size are most probably too large to enable these surfaces to support a composite interface (figure 22a). As previously mentioned, more robust surfaces are obtained with higher density aerogels with a maximum in oleophobicity (166º) at a density of 0.0070 g/cm$^3$ (figure 22d). These properties are probably related to a fine balance between the number of pores, the pore size and the extending sheet-like structures protruding from the surface. In addition, protruding treads of fibril aggregates probably enhance the oleophobic properties. It is assumed that there is no penetration of the oil into the gaps and that the liquid rests on the rough protruding features of the solid material. The air bridging these features then acts as further support for the oil droplet, so that the oil droplet can be considered to sit partly on the solid and partly on air and thus be modeled in the Cassie−Baxter equation.

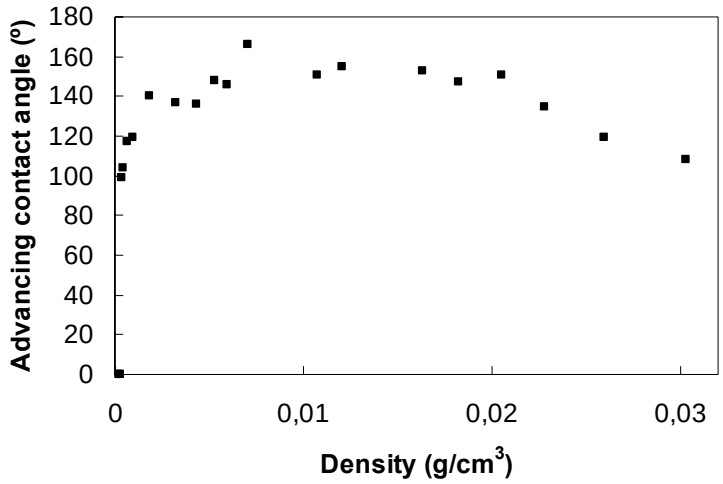


*Figure 29. Advancing contact angle for castor oil as a function of the density of the PFOTS-coated aerogels.*

## 4.5 Microfibrillated cellulose as oil and oxygen barrier for packaging materials (paper V)

As already mentioned, oil resistance of paper products can be achieved in three ways; by refining of the pulp,[21] by chemical treatment of the paper or pulp fibers with low surface

energy fluorocarbons[41, 44] or by applying a barrier on the paper surface.[36, 37] To obtain an oil barrier on more open paper grades, these are generally coated with a polymer. The coating process can replace part of the refining process in the production of oil resistant paper. The oil resistance properties are, from a barrier perspective, a result of the relative absence of pores in the paper and it is controlled by the largest pores.[140] The size of the largest pores and the overall shape of the pore size distribution determine the air permeability of the sheet.[141] Corte et al.[141] reported that small pores with a narrow size distribution result in low air permeability. If these barriers could be extended by coating to include an oxygen barrier, new end-use areas would open up for oil resistant paper. To meet the demand for low oxygen permeability, the coated polymer must meet a number of general criteria. Properties of the polymer film which reduce the permeability are: high crystallinity, low mobility of the polymer chains segments (high cohesive energy density and low free volume) and a dense and tortuous polymer matrix.[142] Since MFC is a semi-crystalline polymer with coexistent phases with different crystallinities, the structure can create some complex transport phenomena. In semi-crystalline polymers, the crystalline regions are considered to be impermeable to gases.[143-145] The partly crystalline microfibrils in combination with the ability of the dried films to form a dense network held together by strong inter-fibrillar hydrogen bonds and van der Waals interactions, i.e. high cohesive energy density, suggest that the films have high potential barrier properties and that they could be an interesting alternative to fossil-based barriers. Due to the rather high degree of crystallinity of MFC, as shown in table 4, the permeability attributed to the amorphous volume is believed to be limited. However, gases may diffuse through MFC films between the voids in the microfibril network. The intra- and intermolecular hydrogen bonding and van der Waals interaction of adjacent MFC fibrils may reduce the chain mobility and thus the penetrant diffusivity.

### 4.5.1 Surface structure and air permeability properties of MFC-coated papers

The air permeability of a coated unbleached paper (wrapping paper without fillers) is shown as a function of the coat weight of MFC in figure 30. At zero MFC coverage or zero coat weight i.e. for the pure unbleached paper, the air permeability was measured to 69000 nm/Pa s. When the coat weight was increased slightly, the air permeability decreased drastically. When the coating was applied using the largest wire diameter rod, the air permeability was found to be 4.8 nm/Pa s. When the paper was coated twice using the largest wire diameter rod to ensure a complete surface coverage of MFC, the air permeability dropped to 0.3 nm/Pa s.

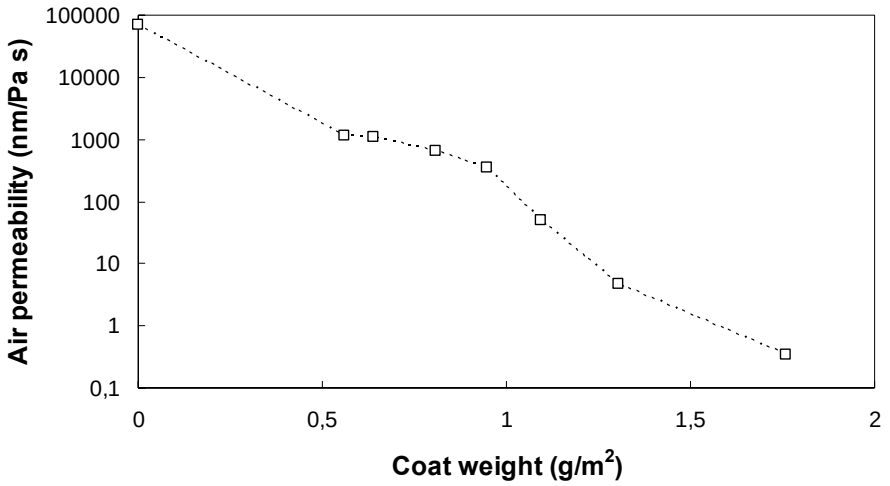

*Figure 30. Air permeability (logarithmic scale) as a function of MFC-coat weight for an unbleached paper coated on a bench scale.*

The surface structures of MFC-coated and uncoated unbleached papers were studied using E-SEM. The results of this study are summarized in figure 31, which shows micrographs of the papers with different coat weights. The unbleached paper (figure 31a) had a very open and porous network of randomly crossed fibers. When the coating weight was increased slightly (figure 31b), the network structure of the paper became less apparent. A further increase in the MFC-coat weight led to film formation of the coating layer (figure 31c), and eventually, when the paper was coated twice (figure 31d), to a hardly visible fibre structure in the base paper. The micrograph shows that the coating had covered the fibers at that coat weight and that the coating then formed a continuous film over the fibers.

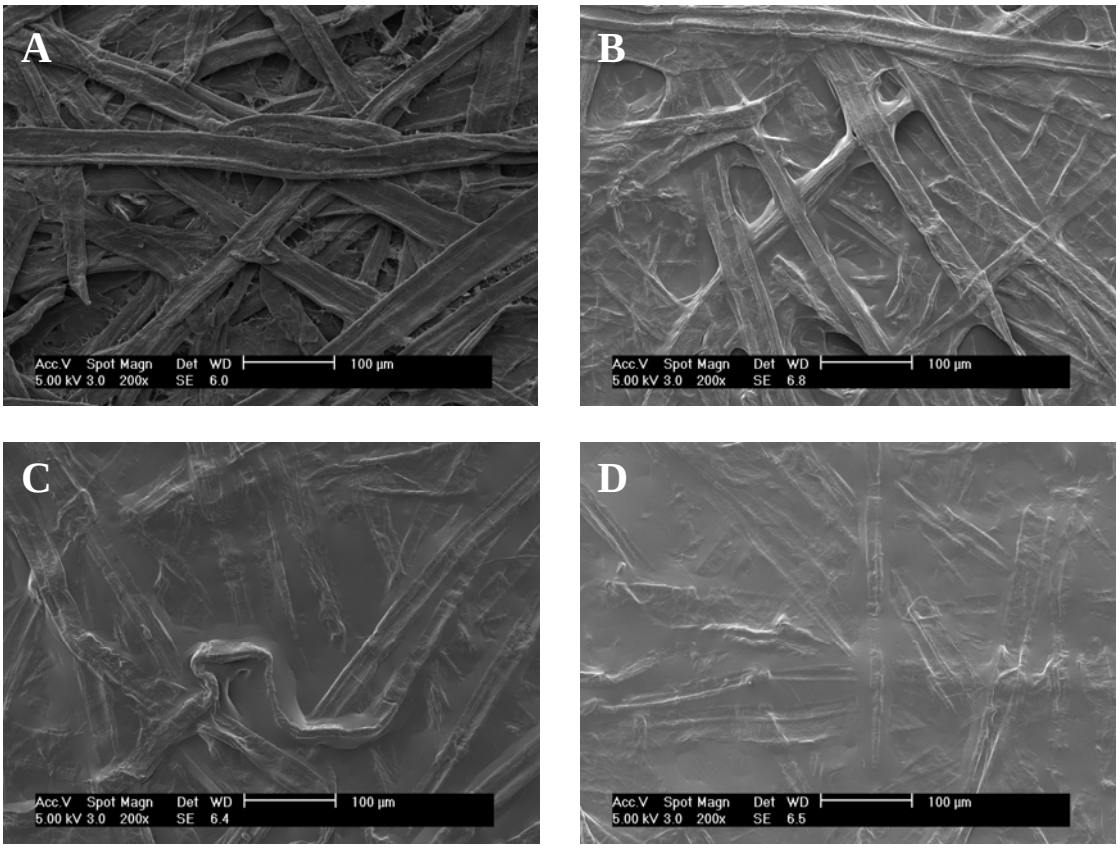


*Figure 31. E-SEM micrographs of (a) uncoated and MFC-coated unbleached papers with coat weights of ca. (b) 0.9, (c) 1.3 and (d) 1.8 g/m$^2$, respectively. The scale bar is 100 µm.*

### 4.5.2 Oil barrier properties of MFC-coated papers

Figure 32 shows the oil resistance of the coated paper as a function of the air permeability. The penetration times of castor oil and turpentine oil are shown. When the air permeability was decreased, the oil resistance increased. It is evident that the coated paper with the lowest air permeability, < 1nm/Pa s, exhibited superior oil resistance (e.g. > 1800 s for castor oil), and that there was a large difference in penetration time between the two oils. The oil penetrated the uncoated unbleached paper immediately (1 s).
The very low air permeability of the coated paper indicates that there are very few connected pores through the whole cross section of the coated paper and that a partly crystalline MFC

layer may form on the paper surface. A crystalline layer in contact with the cellulose fibers is expected to constitute an obstacle for the transport of penetrates, such as turpentine and castor oil, through the coating fiber system and to cause an extension of the diffusion path. The highest coat weight obtained with a single coating was ca 1.3 g/m$^2$. Higher coat weight could not be achieved with a laboratory scale rod coater using a MFC dispersion of 0.85% in the coating. The concentration of the dispersion must be considerably increased if a higher coat weight is to be obtained. An alternative coating technique which yields higher coat weights may also be needed. Curtain or extrusion coating may offer that possibility.[146] The air permeability of the coated material had a great influence on the oil resistance. The air permeability measurements and the oil resistance test showed that MFC can be used as a coating on porous wrapping paper to obtain a material with oil barrier properties, provided that the coating seals the pores in the base paper and forms a continuous and homogeneous film.

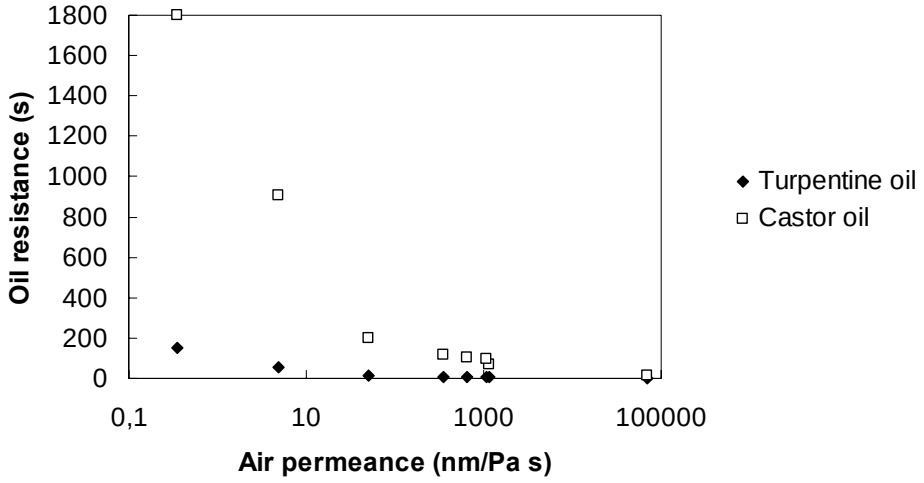


*Figure 32. Oil resistance according to Tappi 454 as a function of air permeability of unbleached paper coated with MFC. Results for castor oil (□) and turpentine oil (♦) are included in the figure. The maximum oil resistance value in the test is 1800 s.*

### 4.5.3 Oxygen barrier properties of MFC films

Two MFC films with grammages of 5 and 8 g/m$^2$ were systematically tested for oxygen transmission rate (OTR) at different relative humidity (RH). When the RH was increased from 0 to 80%, the OTR increased dramatically (figure 33). At RH higher than 70%, the curve became exponential with a sharp increase in permeability. Such behaviour is typical of hydrophilic polymers including cellophane, ethylenevinyl alcohol or wheat gluten films. This exponential effect of RH on OTR was previously observed for other edible film types.[147, 148] and could be related to a sharp increase in polymeric chain mobility.[149] The observed increase in the OTR in the 40−80% RH range is most probably related to the plasticization effect on the amorphous MFC domains of sorbed water molecules. Water molecules in the polymer above a certain water activity level can interact with hydrophilic groups and disrupt hydrogen bonding and van der Waals interactions, creating additional sites for the permeation of oxygen and an increased mobility of oxygen molecules within the polymer network.

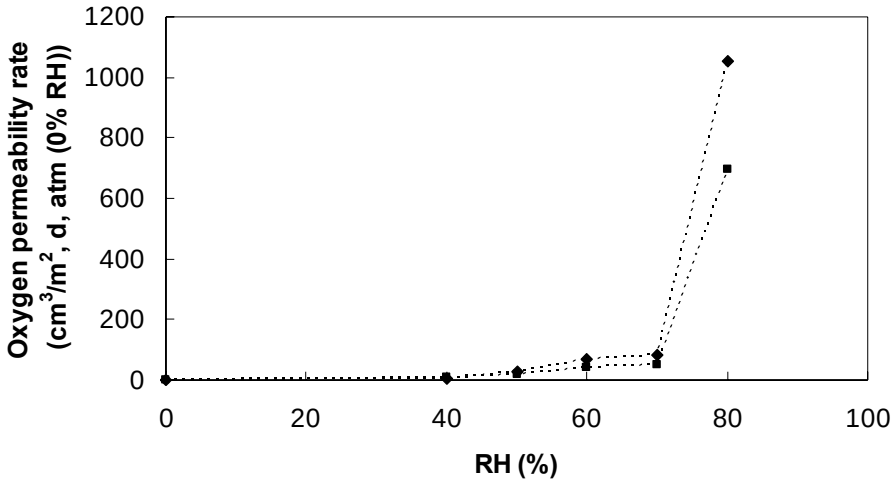


*Figure 33. Effect of relative humidity (% RH) on oxygen transmission rate (OTR) of MFC films with grammages of 5 (♦) and 8 (■) g/m$^2$.*

At 0% RH, MFC films presented very low oxygen permeability values compared to other biodegradable or synthetic films. For example, the oxygen permeability of MFC films at 0% RH was in the same range as that of poly(vinylalcohol) and orders of magnitude lower than that of polyethylene and polystyrene.[150] The measured oxygen permeability at 50% RH is lower than the literature values for glycerol-plasticized starch,[151] whey protein[152] and arabinoxylan.[153]

Apart from the influence of crystallinty, and the ability of the MFC network to form hydrogen bonds and van der Waals interactions, the microstructure of the MFC films is believed to play a significant role for the oxygen permeability properties. Very low film porosity levels are indicated by the FE-SEM micrographs (figure 34). The random orientation and distribution of the nanofibrils is apparent and the thickness of the fibrils was estimated to be ca. 5-10 nm (direct measurements from the FE-SEM image), although larger fibrous entities or cell wall fragments are apparent.

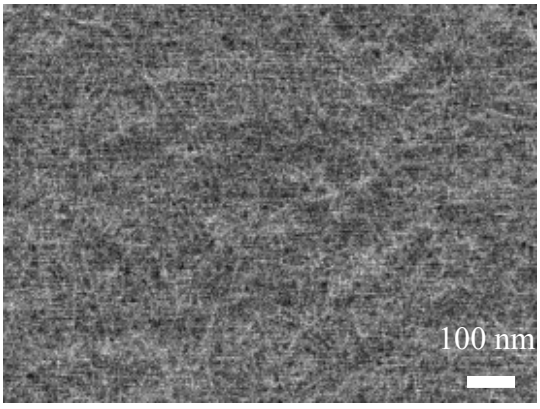


*Figure 34. High-magnification (x30000) FE-SEM image of a MFC film prepared from a dispersion homogenized ten times. The scale bar is 100 nm.*

# 5 Conclusions

A large part of this research was devoted to the development of model cellulose surfaces for studies of wetting by oil mixtures and non-polar liquids. Thin and smooth cellulose model films with different degrees of crystalline ordering were prepared. The studies clearly revealed that cellulose films consisting of low-charged MFC, high-charged MFC and nanocrystals exhibit a cellulose I structure. The cellulose surfaces prepared from dissolving pulp dissolved in NMMO and films prepared by the Langmuir-Schaefer technique exhibit cellulose II ordering whereas the films prepared from LiCl/DMAc have amorphous characteristics with a very low degree of crystalline ordering. The surface morphology of the films was characterized in detail by AFM measurements. The total surface energy of the cellulose films was obtained using contact angle measurements with water, glycerol and diiodomethane. The dispersive contribution to the surface energy was found to dominate the total surface energy of the films.

The build-up of the multilayer films formed by layer-by-layer (LbL) deposition of PEI and MFC was studied in situ by DPI and QCM-D, obtaining complementary information from the two techniques. Large increases in dissipation associated with the adsorption of MFC were obtained by QCM-D. This, together with a registered decrease in refractive index from DPI measurements, indicates that thick and viscous multilayers are formed, with a decrease in average film density for each new layer of MFC adsorbed.

The possibility of creating a multilayer using only charge-stabilized MFC dispersions was established, i.e. the multilayer was composed only of anionically and cationically modified MFC. The build-up behaviour and the properties of the LbL-constructed cellulose films were investigated by combining results from QCM-D and SPAR. The film morphology and surface roughness were studied in detail by AFM. XPS was used to evaluate the surface composition of the films.

In order to obtain oleophobic cellulose films suitable for wetting studies, the prepared surfaces were modified by coating with various amounts of perfluorooctadecanoic acid, or covalently modified with pentadecafluorooctanyl chloride. XPS and dispersive surface energy measurements were made on the cellulose films treated with the fluorinated compounds. An increase in the atomic fluorine concentration yielded a decrease in dispersive surface energy, and thereby an increase in the measured contact angle of the oil mixtures. The viscosity and surface tension of the oils, as well as the dispersive surface energy of the cellulose films, were found to greatly influence the spreading kinetics of the oil mixtures.

A plasma etching approach was made to prepare structured silicon surfaces. The silicon surfaces were coated with cellulose nanocrystals using the LbL technique. The porous structure of the surfaces forms overhang structures and these, combined with the surface free energy of the surfaces, play an important role in inducing the oleophobic properties. After being coated with fluorinated silanes, the porous cellulose surfaces displayed highly non-wetting properties for a number of alkanes with low surface tensions, including hexadecane and decane.

MFC aerogels were successfully prepared by freeze-drying. The microstructure of the porous aerogels was carefully controlled by adjusting the concentration of the MFC dispersion used for the freeze-drying. Different scales of roughness and porosity of the aerogels were utilised, together with the very low surface energy created by fluorination of the aerogel, to induce highly oleophobic properties.

MFC was used to coat thin layers on different base papers. E-SEM micrographs showed that the MFC coatings consisted of randomly assembled nanofibrils, mostly with a thickness of ca. 5-10 nm. The air permeability of the coated paper decreased to a large extent as a result of

MFC coverage. The reduced surface porosity induced by fibrils, as shown by E-SEM, explains the improved oil barrier properties. The MFC coatings are promising for potential applications as transparent and biodegradable packaging films with high barrier properties.

Finally, it should be emphasised that high-resolution techniques together with ordinary paper testing methods have been used to study various cellulose surfaces and paper materials, and for the study of wetting properties on different length scales, from the molecular scale to an open network dimension. A combination of the discussed techniques provides a new important and interesting insight into the mechanisms governing the wetting and spreading of various oils on cellulose materials. Further efforts could concentrate on the application of oleophobic cellulose materials to, for example, textiles, coatings, packaging, micro-fluid channels and chemical industries.

# 6 Acknowledgments

I would like to thank my supervisor, Professor Tom Lindström, for all his support and valuable guidance during my research. Working with you has been truly inspiring.

Professor Lars Wågberg is thanked for allowing me to undertake Ph.D. studies at the Department of Fiber and Polymer Technology at KTH. I am grateful to you for always having been available for discussions and support for my project.

I also want to thank Professor Per Claesson for valuable discussions and for allowing me to use the instruments at the Department of Surface Chemistry.

Professor Lars Ödberg is greatly acknowledged for valuable discussions. I appreciate your help very much.

BIM Kemi AB and the Knowledge Foundation through its graduate school YPK are acknowledged for financial support. BIM has been very kind and supportive to me over the years and always at hand to help me with various matters. I would especially like to thank Mikael Rasmusson, Chris Bonnerup and Mikael Perdin at BIM.

Innventia AB is acknowledged for allowing me to use their facilities and all the kind people who have help me through the years, especially Joanna Hornatowska, Mikael Ankerfors, Åsa Blademo and Gunborg Glad-Nordmark.

Thank you Brita and Inga, for all the help with administrative tasks.

I would like to thank my colleagues in the Fibre Technology Group and at the Department of Fibre and Polymer Technology, especially my closest friends Eva-Helena, Ingemar, Simon, David and Erik.

I would like to take the opportunity to thank my former teachers and friends at Linköping University.

Last but definitely not least; my deepest gratitude goes to my family, especially Sofia, for all their love and support over the years. None of this could have been done without you.

# References


(1) Kontturi, E.; Tammelin, T.; Österberg, M. *Chemical Society Reviews* **2006**, *35*, 1287-1304.
(2) O'Sullivan, A.C. *Cellulose* **1997**, *4*, 173-207.
(3) Paakkari, T.; Serimaa, R.; Fink, H.P. *Acta Polymerica* **1989**, *40*, 731-734.
(4) Michell, A.J.; Higgins, H.G. *Cellulose* **1999**, *6*, 89-91.
(5) Nishiyama, Y.; Langan, P.; Chanzy, H. *Journal of the American Chemical Society* **2002**, *124*, 9074-9082.
(6) Nishiyama, Y.; Okano, T.; Langan, P.; Chanzy, H. *International Journal of Biological Macromolecules* **1999**, *26*, 279-283.
(7) Nishiyama, Y.; Sugiyama, J.; Chanzy, H.; Langan, P. *Journal of the American Chemical Society* **2003**, *125*, 14300-14306.
(8) Wakelyn, P.J. *Handbook of Fiber Chemistry, Cotton Fibers*, 2nd Edition; Marcel Dekker Inc.: NY, 1998.
(9) Boylston, E.K.; Hebert, J.J. *Journal of Applied Polymer Science* **1980**, *25*, 2105-2107.
(10) Zimmerman, T.; Poehler, E.; Geiger, T. *Advanced Engineering Materials* **2004**, *6*, 754-761.
(11) Sarkanen, K.V.; Ludwig, C.H. *Lignins: Occurrence, Formation, Structure and Reactions*, Wiley-Interscience: New York, US, 1971.
(12) Ralph, J.; Brunow, G.; Harris, P.J.; Dixon, R.A.; Schatz, P.F.; Boerjan, W. *Recent Advances in Polyphenol Research* **2008**, *1*, 36-66.
(13) Page, D.H. *Wood and Fiber* **1976**, *7*, 246-248.
(14) Daniel, G.; Volc, J.; Niku-Paavola, M.-L. *Comptes Rendus Biologies* **2004**, *327*, 861-871.
(15) Eklund, D.; Lindström, T. *Paper Chemistry - an introduction*, DT Paper Science Publications: Finland, 1991.
(16) Henriksson, G.; Lawoko, M.; Martin, M.E.E.; Gellerstedt, G. *Holzforschung* **2007**, *61*, 668-674.
(17) Lawoko, M.; Henriksson, G.; Gellerstedt, G. *Biomacromolecules* **2005**, *6*, 3467-3473.
(18) Deisenroth, E.; Jho, C.; Haniff, M.; Jennings, J. *Surface Coatings International* **1998**, *81*, 440-447.
(19) Ham-Pichavant, F.; Sebe, G.; Pardon, P.; Coma, V. *Carbohydrate Polymers* **2005**, *61*, 259-265.
(20) Stolpe, L. *Investigacion y Tecnica del Papel* **1996**, *33*, 415-426.
(21) Kjellgren, H.; Engström, G. *Tappi Journal* **2005**, *4*, 7-11.
(22) Gallay, W. *Theory of the beating process*. *Fundamentals of Papermaking Fibres, Transaction of the Symposium, 377-387.* British Paper and Board Makers Association. Cambridge, UK 1958.
(23) Giertz, H.W. *Effects of beating on individual fibers*. *Fundamentals of Papermaking Fibres, Transaction of the Symposium, 389-409.* British Paper and Board Makers Association. Cambridge, UK 1958.
(24) Scallan, A.M. *The accommodation of water within pulp fibers*. *Fibre-Water Interactions in Paper-Making: Sixth Fundamental research Symposium, Session 1, 9-29*. Oxford, UK 1978.
(25) Scallan, A.M. *Wood Science* **1974**, *6*, 266-271.
(26) Giatti, R. *Investigacion y Tecnica del Papel* **1996**, *33*, 401-414.
(27) Schwartz, C. *Oil resistance utilizing fluorochemicals*. *Technical Association of the Pulp and Paper Industry, Section Sizing*. Tappi Press. Chicago, US 1981.

(28) Dill, D.R. *Tappi* **1974**, *57*, 97-100.
(29) Hoyland, R.W.; Field, R. *A review of the transudation of water into paper - in five parts. Part 5: The mechanism of penetration, and conclusions*. *Paper Technology and Industry*. Manchester, UK 1977.
(30) Klass, C.P. *Development and applications of the metered size press*. *TAPPI Metered Size Press Forum*. TAPPI Press. Orlando, US 2002.
(31) Michelman, J.S.; Homoelle, J.B. *Tappi Journal* **1989**, *72*, 159-163.
(32) Yeates, S.G.; Passier, H.; Satguru, R.; Farrar, J. *European Coatings Journal* **1996**, 294, 296-298.
(33) Rissa, K.; Vähä-Nissi, M.; Lepisto, T.; Savolainen, A. *Paperi ja Puu* **2002**, *84*, 467-472.
(34) Vähä-Nissi, M.; Savolainen, A. *Filled barrier dispersion coatings*. *TAPPI Coating Conference*. TAPPI Press. Toronto, Canada 1999.
(35) Tsunemitsu, K.; Murakami, Y. *Use of poly(vinyl alcohol) in paper manufacture*, John Wiley & Sons: UK, 1973.
(36) Krook, M.; Gällstedt, M.; Hedenqvist, M.S. *Packaging Technology & Science* **2005**, *18*, 11-20.
(37) Gross, R.A.; Kalra, B. *Science* **2002**, *297*, 803-807.
(38) Kissa, E. *Fluorinated Surfactants and Repellents, Revised and Expanded*, 2nd Edition; Marcel Dekker: New York, 2001.
(39) Rojas, O.J.; Macakova, L.; Blomberg, E.; Emmer, A.; Claesson, P.M. *Langmuir* **2002**, *18*, 8085-8095.
(40) Schoenroth, K.G.; Rengel, G.L. *Pulp & Paper Magazine of Canada* **1967**, *68*, 478-480.
(41) Fukuda, S.; Isogai, A.; Kitaoka, T.; Sumikawa, N. *Nordic Pulp & Paper Research Journal* **2005**, *20*, 496-501.
(42) Liu, Y.; Jho, C. *Journal of Pulp and Paper Science* **2004**, *30*, 45-49.
(43) Rengel, G.L.; Perrault, E.W.; Rambosek, G.M. *Tappi* **1966**, *49*, 76-79.
(44) Yang, L.; Pelton, R.; McLellan, F.; Fairbank, M. *Tappi Journal* **1999**, *82*, 128-135.
(45) Hayek, M. *Waterproofing and water/oil repellency*, 3rd Edition; New York, US, 1983.
(46) Luner, P.; Sandell, M. *Journal of Polymer Science, Polymer Symposia* **1969**, *28*, 115-142.
(47) Schaub, M.; Wenz, G.; Wegner, G.; Stein, A.; Klemm, D. *Advanced Materials* **1993**, *5*, 919-922.
(48) Buchholz, V.; Wegner, G.; Stemme, S.; Ödberg, L. *Advanced Materials* **1996**, *8*, 399-402.
(49) Fält, S.; Wågberg, L.; Vesterlind, E.L.; Larsson, P.T. *Cellulose* **2004**, *11*, 151-162.
(50) Eriksson, J.; Malmsten, M.; Tiberg, F.; Callisen, T.H.; Damhus, T.; Johansen, K.S. *Journal of Colloid and Interface Science* **2005**, *284*, 99-106.
(51) Eriksson, M.; Notley, S.M.; Wågberg, L. *Biomacromolecules* **2007**, *8*, 912-919.
(52) Notley, S.M.; Eriksson, M.; Wågberg, L.; Beck, S.; Gray, D.G. *Langmuir* **2006**, *22*, 3154-3160.
(53) Fält, S.; Wågberg, L.; Vesterlind, E.-L. *Langmuir* **2003**, *19*, 7895-7903.
(54) Aulin, C.; Shchukarev, A.; Lindqvist, J.; Malmström, E.; Wågberg, L.; Lindström, T. *Journal of Colloid and Interface Science* **2008**, *317*, 556-567.
(55) Gunnars, S.; Wågberg, L.; Cohen Stuart, M.A. *Cellulose* **2002**, *9*, 239-249.
(56) Aulin, C.; Ahola, S.; Josefsson, P.; Nishino, T.; Hirose, Y.; Österberg, M.; Wågberg, L. *Langmuir* **2009**, *25*, 7675-7685.
(57) Notley, S.M.; Wågberg, L. *Biomacromolecules* **2005**, *6*, 1586-1591.
(58) Edgar, C.D.; Gray, D.G. *Cellulose* **2003**, *10*, 299-306.

(59) Cranston, E.D.; Gray, D.G. *Biomacromolecules* **2006**, *7*, 2522-2530.
(60) Notley, S.M.; Norgren, M. *Langmuir* **2006**, *22*, 11199-11204.
(61) Kontturi, E.; Johansson, L.-S.; Kontturi, K.S.; Ahonen, P.; Thuene, P.C.; Laine, J. *Langmuir* **2007**, *23*, 9674-9680.
(62) Wågberg, L.; Decher, G.; Norgren, M.; Lindström, T.; Ankerfors, M.; Axnäs, K. *Langmuir* **2008**, *24*, 784-795.
(63) Gavillon, R.; Budtova, T. *Biomacromolecules* **2008**, *9*, 269-277.
(64) Jin, H.; Nishiyama, Y.; Wada, M.; Kuga, S. *Colloids and Surfaces, A: Physicochemical and Engineering Aspects* **2004**, *240*, 63-67.
(65) Svagan, A.J.; Samir, M.A.S.A.; Berglund, L.A. *Advanced Materials* **2008**, *20*, 1263-1269.
(66) Pääkkö, M.; Vapaavuori, J.; Silvennoinen, R.; Kosonen, H.; Ankerfors, M.; Lindström, T.; Berglund, L.A.; Ikkala, O. *Soft Matter* **2008**, *4*, 2492-2499.
(67) Young, T. *Philosophical Transactions of the Royal Society London* **1805**, *95*, 65.
(68) Wenzel, R.N. *Journal of Industrial and Engineering Chemistry* **1936**, *28*, 988-994.
(69) Cassie, A.B.D.; Baxter, S. *Transactions of the Faraday Society* **1944**, *40*, 546-551.
(70) Werner, O.; Wågberg, L.; Lindström, T. *Langmuir* **2005**, *21*, 12235-12243.
(71) Tuteja, A.; Choi, W.; Ma, M.; Mabry, J.M.; Mazzella, S.A.; Rutledge, G.C.; McKinley, G.H.; Cohen, R.E. *Science* **2007**, *318*, 1618-1622.
(72) Cao, L.; Hu, H.-H.; Gao, D. *Langmuir* **2007**, *23*, 4310-4314.
(73) Nosonovsky, M. *Langmuir* **2007**, *23*, 3157-3161.
(74) Cao, L.; Price, T.P.; Weiss, M.; Gao, D. *Langmuir* **2008**, *24*, 1640-1643.
(75) Washburn, E.W. *Physical Review* **1921**, *17*, 374-375.
(76) Cao, A.; Cao, L.; Gao, D. *Applied Physics Letters* **2007**, *91*, 034102/1-034102/3.
(77) Erbil, H.Y.; Demirel, A.L.; Avci, Y.; Mert, O. *Science* **2003**, *299*, 1377-1380.
(78) Marmur, A. *Langmuir* **2004**, *20*, 3517-3519.
(79) Lafuma, A.; Quere, D. *Nature Materials* **2003**, *2*, 457-460.
(80) Yabu, H.; Takebayashi, M.; Tanaka, M.; Shimomura, M. *Langmuir* **2005**, *21*, 3235-3237.
(81) Miwa, M.; Nakajima, A.; Fujishima, A.; Hashimoto, K.; Watanabe, T. *Langmuir* **2000**, *16*, 5754-5760.
(82) Yoshimitsu, Z.; Nakajima, A.; Watanabe, T.; Hashimoto, K. *Langmuir* **2002**, *18*, 5818-5822.
(83) Feng, L.; Li, S.; Li, Y.; Li, H.; Zhang, L.; Zhai, J.; Song, Y.; Liu, B.; Jiang, L.; Zhu, D. *Advanced Materials* **2002**, *14*, 1857-1860.
(84) Onda, T.; Shibuichi, S.; Satoh, N.; Tsujii, K. *Langmuir* **1996**, *12*, 2125-2127.
(85) Reynolds, W.F. *The Sizing of Paper*, 2nd edition; Tappi Press: US, 1989.
(86) Kjellgren, H.; Engström, G. *Nordic Pulp & Paper Research Journal* **2006**, *21*, 685-689.
(87) Kjellgren, H.; Gällstedt, M.; Engsträm, G.; Järnström, L. *Carbohydrate Polymers* **2006**, *65*, 453-460.
(88) Winnik, M.A.; Bystryak, S.M.; Chassenieux, C.; Strashko, V.; Macdonald, P.M.; Siddiqui, J. *Langmuir* **2000**, *16*, 4495-4510.
(89) Meszaros, R.; Thompson, L.; Varga, I.; Gilanyi, T. *Langmuir* **2003**, *19*, 9977-9980.
(90) Meszaros, R.; Varga, I.; Gilanyi, T. *Langmuir* **2004**, *20*, 5026-5029.
(91) Diddens, I.; Murphy, B.; Krisch, M.; Mueller, M. *Macromolecules* **2008**, *41*, 9755-9759.
(92) Herrick, F.W.; Casebier, R.L.; Hamilton, J.K.; Sandberg, K.R. *Journal of Applied Polymer Science: Applied Polymer Symposium* **1983**, *37*, 797-813.

(93) Turbak, A.F.; Snyder, F.W.; Sandberg, K.R. *Journal of Applied Polymer Science: Applied Polymer Symposium* **1983**, *37*, 815-827.
(94) Pääkkö, M.; Ankerfors, M.; Kosonen, H.; Nykänen, A.; Ahola, S.; Österberg, M.; Ruokolainen, J.; Laine, J.; Larsson, P.T.; Ikkala, O.; Lindström, T. *Biomacromolecules* **2007**, *8*, 1934-1941.
(95) Winter, L.; Wågberg, L.; Ödberg, L.; Lindström, T. *Journal of Colloid and Interface Science* **1986**, *111*, 537-543.
(96) Berthold, F.; Gustafsson, K.; Berggren, R.; Sjöholm, E.; Lindström, M. *Journal of Applied Polymer Science* **2004**, *94*, 424-431.
(97) Dong, X.M.; Kimura, T.; Revol, J.-F.; Gray, D.G. *Langmuir* **1996**, *12*, 2076-2082.
(98) Tammelin, T.; Saarinen, T.; Österberg, M.; Laine, J. *Cellulose* **2006**, *13*, 519-535.
(99) Ahola, S.; Salmi, J.; Johansson, L.S.; Laine, J.; Österberg, M. *Biomacromolecules* **2008**, *9*, 1273-1282.
(100) Thuenemann, A.F.; Schnablegger, H. *Langmuir* **1999**, *15*, 5426-5428.
(101) Nyström, D.; Lindqvist, J.; Östmark, E.; Hult, A.; Malmström, E. *Chemical Communications* **2006**, 3594-3596.
(102) Jasper, J.J. *Journal of Physical and Chemical Reference Data* **1972**, *1*, 841-1009.
(103) Asthana, S.K.; Koteswara Rao, M.V.R.; Balakrishna, K.J. *Perfumery and Essential Oil Record* **1964**, *55*, 725-727.
(104) Briggs, D.; Grant, J.T. *Surface Analysis by Auger and X-Ray Photoelectron Spectroscopy*, Wiley Interscience: Chichester, UK, 2003.
(105) Zhong, Q.; Inniss, D.; Kjoller, K.; Elings, V.B. *Surface Science* **1993**, *290*, 688-692.
(106) Binnig, G.; Gerber, C.; Stoll, E.; Albrecht, T.R.; Quate, C.F. *Europhysics Letters* **1987**, *3*, 1281-1286.
(107) Van Oss, C.J.; Ju, L.; Chaudhury, M.K.; Good, R.J. *Journal of Colloid and Interface Science* **1989**, *128*, 313-319.
(108) Van Oss, C.J. *Interfacial Forces in Aqueous Media*, Marcel Dekker: New Work, US, 1994.
(109) Rodahl, M.; Hook, F.; Krozer, A.; Brzezinski, P.; Kasemo, B. *Review of Scientific Instruments* **1995**, *66*, 3924-3930.
(110) Enarsson, L.-E. *Ph.D. Thesis*, Royal Institute of Technology: Stockholm, 2008.
(111) Dijt, J.C.; Stuart, M.A.C.; Hofman, J.E.; Fleer, G.J. *Colloids and Surfaces* **1990**, *51*, 141-158.
(112) Dijt, J.C.; Cohen Stuart, M.A.; Fleer, G.J. *Advances in Colloid and Interface Science* **1994**, *50*, 79-101.
(113) Azzam, R.M.A.; Bashara, N.M. *Ellipsometry and Polarized Light*, Elsevier North Holland: US, 1977.
(114) Lu, J.R.; Swann, M.J.; Peel, L.L.; Freeman, N.J. *Langmuir* **2004**, *20*, 1827-1832.
(115) Zhao, X.; Pan, F.; Coffey, P.; Lu, J.R. *Langmuir* **2008**, *24*, 13556-13564.
(116) Lee, L.; Johnston, A.P.R.; Caruso, F. *Biomacromolecules* **2008**, *9*, 3070-3078.
(117) Sonesson, A.W.; Callisen, T.H.; Brismar, H.; Elofsson, U.M. *Colloids and Surfaces, B: Biointerfaces* **2007**, *54*, 236-240.
(118) Halthur, T.J.; Claesson, P.M.; Elofsson, U.M. *Langmuir* **2006**, *22*, 11065-11071.
(119) Swann, M.J.; Peel, L.L.; Carrington, S.; Freeman, N.J. *Analytical Biochemistry* **2004**, *329*, 190-198.
(120) Freeman, N.J.; Peel, L.L.; Swann, M.J.; Cross, G.H.; Reeves, A.; Brand, S.; Lu, J.R. *Condensed Matter* **2004**, *16*, 2493-2496.
(121) Raghavan, D.; Gu, X.; Nguyen, T.; VanLandingham, M.; Karim, A. *Macromolecules* **2000**, *33*, 2573-2583.

(122) Bar, G.; Thomann, Y.; Brandsch, R.; Cantow, H.J.; Whangbo, M.H. *Langmuir* **1997**, *13*, 3807-3812.
(123) Forsström, J.; Eriksson, M.; Wågberg, L. *Journal of Adhesion Science and Technology* **2005**, *19*, 783-798.
(124) Berg, J.C. *Nordic Pulp & Paper Research Journal* **1993**, *8*, 75-85.
(125) Luner, P.E.; Oh, E. *Colloids and Surfaces, A: Physicochemical and Engineering Aspects* **2001**, *181*, 31-48.
(126) Berg, J.C. *Role of acid-base interactions in wetting and related phenomena*, Marcel Dekker: New York, US, 1993.
(127) Toussaint, A.F.; Luner, P. *Journal of Adhesion Science and Technology* **1993**, *7*, 635-648.
(128) Patterson, A.L. *Physical Review* **1939**, *56*, 978-982.
(129) Decher, G. *Science* **1997**, *277*, 1232-1237.
(130) Meszaros, R.; Thompson, L.; Bos, M.; de Groot, P. *Langmuir* **2002**, *18*, 6164-6169.
(131) De Feijter, J.A.; Benjamins, J.; Veer, F.A. *Biopolymers* **1978**, *17*, 1759-1772.
(132) Sauerbrey, G. *Zeitschrift fuer Physik* **1959**, *155*, 206-222.
(133) Mezei, A.; Meszaros, R.; Varga, I.; Gilanyi, T. *Langmuir* **2007**, *23*, 4237-4247.
(134) Meszaros, R.; Thompson, L.; Bos, M.; Varga, I.; Gilanyi, T. *Langmuir* **2003**, *19*, 609-615.
(135) Bogue, R. *Sensor Review* **2002**, *22*, 41-45.
(136) Hare, E.F.; Shafrin, E.G.; Zisman, W.A. *Journal of Physical Chemistry* **1954**, *58*, 236-239.
(137) Holmberg, K.; Lindman, B.; Jönsson, B.; Kronberg, B. *Surfactants and Polymers in Aqueous Solution,* , 2nd Edition; John Wiley & Sons: Chichester, UK, 2002.
(138) He, B.; Patankar, N.A.; Lee, J. *Langmuir* **2003**, *19*, 4999-5003.
(139) Zimmermann, J.; Rabe, M.; Artus, G.R.J.; Seeger, S. *Soft Matter* **2008**, *4*, 450-452.
(140) Corte, H.; Lloyd, E.H. *Fluid flow through paper and sheet structure*. *Consolidation of the Paper Web, Transactions of the Symposium, Section 2, 981-1009*. Wiggins Teape. Cambridge, UK 1966.
(141) Corte, H. *Porous structure of paper*. *Fundamentals of Papermaking Fibres, Transaction of the Symposium, 301-331.* British Paper and Board Makers Association. Cambridge, UK 1958.
(142) Ito, K.; Saito, Y.; Yamamoto, T.; Ujihira, Y.; Nomura, K. *Macromolecules* **2001**, *34*, 6153-6155.
(143) Furuheim, K.M.; Axelson, D.E.; Helle, T. *Nordic Pulp & Paper Research Journal* **2003**, *18*, 168-175.
(144) Arvanitoyannis, I.; Kalichevsky, M.; Blanshard, J.M.V.; Psomiadou, E. *Carbohydrate Polymers* **1994**, *24*, 1-15.
(145) Stern, S.A.; Shah, V.M.; Hardy, B.J. *Journal of Polymer Science, Part B: Polymer Physics* **1987**, *25*, 1263-1298.
(146) Kjellgren, H.; Gällstedt, M.; Engström, G.; Järnström, L. *Carbohydrate Polymers* **2006**, *65*, 453-460.
(147) McHugh, T.H.; Krochta, J.M. *Journal of Agricultural and Food Chemistry* **1994**, *42*, 841-845.
(148) Gontard, N.; Thibault, R.; Cuq, B.; Guilbert, S. *Journal of Agricultural and Food Chemistry* **1996**, *44*, 1064-1069.
(149) Gontard, N.; Guilbert, S.; Cuq, J.L. *Journal of Food Science* **1992**, *57*, 190-195, 199.
(150) Lange, J.; Wyser, Y. *Packaging Technology & Science* **2003**, *16*, 149-158.
(151) Rindlav-Westling, A.; Stading, M.; Hermansson, A.-M.; Gatenholm, P. *Carbohydrate Polymers* **1998**, *36*, 217-224.

(152) Sothornvit, R.; Krochta, J.M. *Journal of Agricultural and Food Chemistry* **2000**, *48*, 3913-3916.
(153) Höije, A.; Sternemalm, E.; Heikkinen, S.; Tenkanen, M.; Gatenholm, P. *Biomacromolecules* **2008**, *9*, 2042-2047.